Journal of Sound and Vibration 548 (2023) 117526

Contents lists available at ScienceDirect

Journal of Sound and Vibration

journal homepage: www.elsevier.com/locate/jsvi

Modeling of geometrical stiffening in a rotating blade—A review

Lokanna Hoskoti [a], Shakti S. Gupta [b], Mahesh M. Sucheendran [a,*]

[a] Mechanical and Aerospace Engineering, Indian Institute of Technology Hyderabad, 502284, India
[b] Mechanical Engineering, Indian Institute of Technology Kanpur, 208016, India

ARTICLE INFO

Keywords:
Pre-twisted rotating Timoshenko beams
Hybrid deformation variables
Geometrical/centrifugal stiffening
Cantilever beam vibration
Rayleigh method
Bending–bending–torsion coupling
Linear and nonlinear vibration

ABSTRACT

The present work reviews different approaches adopted for modeling the geometrical or centrifugal stiffening of a beam due to rotation about an axis perpendicular to its longitudinal axis. The longitudinal displacement of the beam consists of three components: the axial displacement of the neutral axis (elastic extension), displacement associated with rotation of the plane section and the displacement due to the foreshortening effect. A widely used approach for modeling the geometrical stiffening is based on the foreshortening effect, which essentially is the longitudinal shrinkage due to the transverse motion of the beam. This approach uses nonlinear strain–displacement relations. As a result, the equations of motion and associated boundary conditions are nonlinear. The geometric stiffening terms in the nonlinear models are fundamentally a linear/quadratic function of the high-frequency axial elastic deformation. Various nonlinear models are discussed and summarized based on the different approximations of the strain–displacement relation. The solution procedure of these nonlinear models is complicated and computationally expensive due to coupling between high-frequency axial and low-frequency bending modes. Simplifying the model by direct linearization of the equations of motion eliminates the geometrical stiffening term resulting in an incorrect model. Different approaches to include geometrical stiffening terms in the linear model are discussed. One of the approaches is linearizing the nonlinear terms arising from the coupled axial-transverse motion around the steady-state axial solutions. The steady-state axial equilibrium equation can be linear or nonlinear depending on the type of strain measure employed. A comparison of the solution of these different linear/nonlinear steady-state axial equilibrium equations is presented. The applicability of these models based on the steady-state axial equations is tested, and the rotation speed limit within which these models are valid is also discussed. In another approach, the equations of motion are derived using a time-independent centrifugal force. The resulting equations are equivalent to those governing the transverse vibrations of beams subject to an external axial force. Nevertheless, another approach proposed by Kane et al. (1987) uses stretch as a variable in the formulation instead of the axial displacement. The linear geometrical stiffening models are discussed in detail. Further, the effects of geometric properties of the blade, such as taper, twist angle, pre-setting angle and asymmetry in cross-section on the modal characteristics are brought out. A comparison of the different beam theories used in studying the dynamics of rotating blades is also presented.

* Corresponding author.
E-mail address: mahesh@mae.iith.ac.in (M.M. Sucheendran).

https://doi.org/10.1016/j.jsv.2022.117526
Received 20 September 2022; Received in revised form 29 November 2022; Accepted 15 December 2022
Available online 19 December 2022

1. Introduction

A pre-twisted and tapered cantilever beam with an asymmetric cross-section mounted on a rotating hub with some setting angle under aerodynamic excitation can be a simple model to study the dynamics of a free-standing rotating blade in helicopters/wind turbines/ turbomachinery [1]. During the last five decades, numerous authors have published papers on the dynamic analysis of a rotating blade idealized using simplified one-dimensional analytical models based on Euler–Bernoulli and Timoshenko beam theories with varying levels of complexity in geometry.

The dynamic features of a rotating blade vary significantly from that of a stationary blade due to the rotation-induced effects such as *Coriolis force* and *centrifugal force*. A rotating blade experiences Coriolis force when the blade is experiencing an axial deformation. The Coriolis force acts perpendicular to the direction of the axial deformation and the axis of rotation. At sufficiently high speeds, the effect of Coriolis force, also known as the gyroscopic coupling effect, is significant. This force is proportional to the rotation velocity and time derivative of the elastic deformations. The gyroscopic coupling terms appear identical to the damping terms in the linear eigenvalue problem. However, unlike damping forces, the Coriolis force forms a skew-symmetric matrix. The centrifugal forces resulting from the rotation that acts in the blade's axial direction lead to the higher bending stiffness of the beam than a non-rotating beam. This geometric stiffening effect due to rotation is referred to in the literature as centrifugal stiffening. Some other terminologies used for the effect are stress stiffening, geometric stiffening, rotational stiffening and dynamic stiffening [2]. Extensive research has been conducted in the past in order to account for this effect properly.

Modeling of geometrical stiffening of rotating beams has been of interest to many researchers during the last few decades. Various approaches have been used to model this effect. One of the widely used models is based on the foreshortening effect. The second-degree foreshortening terms due to bending motion are included either implicitly or explicitly. The geometrical stiffening models based on implicit foreshortening include the work done by the centrifugal force [3,4]. Further, when foreshortening is modeled implicitly, the modeling requires the use of the nonlinear strain–displacement relation. The resulting nonlinear equations of motion may be linearized in different ways. The explicit geometrical stiffening models use an axial displacement field that includes the second-degree foreshortening terms and employ nonlinear strain–displacement relations. The linear equations of motion are obtained by neglecting the third and higher-order terms in the kinetic and potential energy expressions. As a result of using foreshortening explicitly in the axial displacement field, the geometrical stiffening terms appear in the final equations through the kinetic energy rather than through the potential energy as in the implicit geometrical stiffening models [3]. The implicit and explicit methods describe the longitudinal displacement using the coordinates of a material point before or after deformation, respectively. Some authors use stretch as a variable in place of longitudinal displacement, which is measured using coordinates after deformation [5,6]. In contrast, others described the conventional way of measuring the displacement using the coordinates before deformation [7]. Detailed discussion about these models in terms of the geometric stiffening effect is presented in [8] and compared the differences among the other modeling methods. Few more review papers discuss various models accounting for the geometrical stiffening effect in which the significance of different nonlinear terms in strain–displacement relation is quantified [4,7,9]. In such a model, the geometric stiffening term is a function of elastic displacements. Other models are based on directly providing nonlinear/linear, time-independent axial force (centrifugal) due to angular velocity [10,11]. Some other approaches to account for nonlinear geometric effects are introduced based on the Substructuring Technique [2,12]. In such an approach, the rotating blade is partitioned into several linear flexible substructures with a local reference frame attached to it. The deformation of each substructure is defined with respect to the local reference frame. Each substructure has small deformations, but several substructures combined will have large deformations.

The vibration characteristics of a rotating blade also vary with geometric properties of the blade, such as *taper, twist angle* and *asymmetry in cross-section*. Due to considerable changes in the mass and stiffness distributions, the blade taper significantly influences its vibration characteristics. The pre-twisting of the blade causes the coupling between the bending motions. Further, the coupled bending and torsional motion occur due to an asymmetric cross-section in which the elastic axis does not coincide with the centroidal axis. The elastic axis is the line that passes through the elastic center about which the applied transverse loads produce only bending unaccompanied by torsion. In contrast, the centroidal axis is the line that passes through the centroid of the cross-sections of the blade. The blade is mounted on the rotating hub such that the chord makes an angle with the engine axis, generally known as *pre-setting* or *staggered angle*. Due to this angle, the equations governing the axial and bending motions are coupled. Dynamic analysis of the rotating blade is further complicated by secondary effects such as *shear deformation, rotary inertia* and *warping of cross-section*. Therefore, the equations of the motion for a rotating blade modeled using the Timoshenko beam with cantilever boundary conditions consist of six-coupled partial differential equations; one for the axial motion, two for the bending motions, two for the shear deformations, and one for the torsion motion.

Some review papers on the vibration characteristics of rotating blades are [13–15]. Some recently published papers covering detailed surveys on rotating-beam dynamics are [16–18]. Doctoral theses that provide state-of-the-art on the subject are [19–22]. A few selective papers that provide further references are [23,24]. Modeling of the rotor blade using a thin-walled beam made of the composite material is covered in survey papers [25,26] and books [27–29]. Further, literature is available on rotating-beam made of functionally graded materials [30–33]. Many review papers on layer-wise theories for the vibration of rotating composite anisotropic blades have been published [34,35]. Considerable literature is available on the dynamics of the blade modeled as plate [36–39] or shell [40–43].

To the best of the authors' knowledge, a survey and comparison of the linear and nonlinear geometrical stiffening models are not discussed extensively in the available literature. The present paper attempts to fill this gap. The detailed survey on implicit and

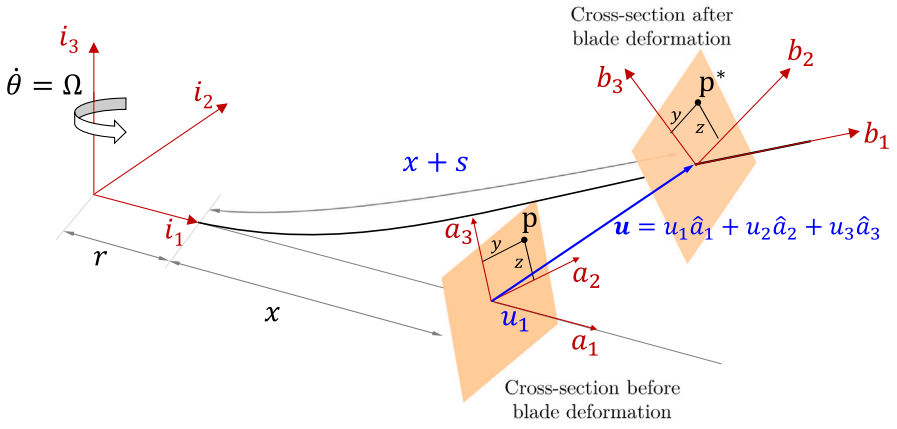

Fig. 1. A simple model of a rotating beam.

explicit methods and the applicability of these models for the rotating blade are discussed. Further, a detailed review of the effect of the rotation, geometric properties and higher-order effects on the modal characteristics of a rotating blade is presented.

This paper is organized as follows. In Section 2, the kinematics description of a rotating blade, including different representations of the rigid body transformation (rotation) matrix, is presented. The expression for kinetic and strain energies are derived for a general case of a rotating blade approximated as a beam. In Section 3, linear and nonlinear geometrical stiffening models and their comparison is presented. The applicability of linear models in the rotation speed range is discussed. In Section 4, different approaches for deriving equations of motion and the solution procedure used for a rotating blade problem are presented. In Section 5, the effect of the blade geometry, rotation, and comparison of different beam theories used to approximate the blade are elaborated, followed by the conclusion in Section 6.

2. Kinematics of a rotating blade

Notations. A standard notation for scalar, vector and matrix is adopted throughout the paper. A small bold letter represents a vector with its components in unbold letters. A capital bold and unbold letter indicates the matrix and its components, respectively. The coordinate system is represented by the small bold letter with a hat over it and the unit vectors are represented by the unbold letter with the hat. For instance, A coordinate frames of reference $\hat{\mathbf{a}}$ has its three mutually perpendicular unit vectors $\{\hat{a}\} = \begin{pmatrix}\hat{a}_1 & \hat{a}_2 & \hat{a}_3\end{pmatrix}^T$ or $\hat{a}_i$, where, i is an index which runs from 1 to 3 in a Euclidean space, i.e., $i = 1, 2, 3$ and $()^T$ indicate the transpose throughout the document. A vector $\mathbf{a}$ has its components a_i or $\{a\} = \begin{pmatrix}a_1 & a_2 & a_3\end{pmatrix}^T$. Similarly, a matrix $\mathbf{A}$ has its components A_{ij} or $[A] = \begin{pmatrix}A_{11} & A_{12} & A_{13}\\ A_{21} & A_{22} & A_{23}\\ A_{31} & A_{32} & A_{33}\end{pmatrix}$. The dot and cross product of any two vectors $\mathbf{a}$ and $\mathbf{b}$ are given by $\mathbf{ab} = a_i b_i$ and $\mathbf{a}\times\mathbf{b} = \begin{pmatrix}a_2b_3 - a_3b_2\\ a_3b_1 - a_1b_3\\ a_1b_2 - a_2b_1\end{pmatrix}$, respectively. The cross product is also a vector and can be expressed as a linear transformation $\mathbf{a}\times\mathbf{b} = \tilde{\mathbf{a}}\mathbf{b} = -\tilde{\mathbf{b}}\mathbf{a}$, where, $\tilde{()}$ is the Cross Product Operator (CPO). The CPO of a vector, $\mathbf{a}$, is given by $[\tilde{a}] = \begin{bmatrix}0 & -a_3 & a_2\\ a_3 & 0 & -a_1\\ -a_2 & a_1 & 0\end{bmatrix}$. A linear transformation of a vector, $\mathbf{a}$, into another vector, $\mathbf{b}$ is given by $\mathbf{a} = \mathbf{Ab}$ or $a_i = A_{ij}b_j$, where, $\{a\}$ and $\{b\}$ are column vectors and $[A]$ is the square matrix. The product of two matrices $\mathbf{A}$ and $\mathbf{B}$ is given by $\mathbf{C} = \mathbf{AB}$ or $C_{ij} = A_{ik}B_{kj}$. With standard notation in mind, the mathematical model of a rotating blade and its kinematics is presented in the following section.

A simple multibody system that consists of a deformable cantilever beam attached to a rigid hub of radius, r, rotating with angular velocity, $\dot{\theta} = \Omega$ is shown in Fig. 1. Three different coordinate frames of reference are introduced to describe the motion of the blade. The inertial frame, $\hat{\mathbf{i}}$, the body frame, $\hat{\mathbf{a}}$, and the local frame, $\hat{\mathbf{b}}$, as shown in Fig. 1 are used to determine the kinematics of a material particle of the blade. The frame, $\hat{\mathbf{i}}$, is attached to the center of the hub with unit vectors $\hat{i}_k$. Unit vector $\hat{i}_1$ is along the length, parallel to the elastic axis of the blade. The hub rotates about $\hat{i}_3$ axis with angular velocity Ω. The unit vector $\hat{i}_2$ is perpendicular to the rotating axis of the rigid hub. The body frame, $\hat{\mathbf{a}}$, is attached to a point on the elastic axis of the un-deformed blade whose unit vectors are $\hat{a}_k$. Here, $\hat{a}_1$ is along the blade span, whereas $\hat{a}_2$ and $\hat{a}_3$ are the principal axes of the cross-section of the undeformed blade. The local frame, $\hat{\mathbf{b}}$ with unit vectors $\hat{b}_k$ is introduced to measure the deformation of the blade as shown in Fig. 1. The unit vector $\hat{b}_1$ is along the tangent to the elastic axis and while $\hat{b}_2$ and $\hat{b}_3$ are the principal axes of the deformed cross-section. Consider an arbitrary point, $\mathbf{p}$, located at $\mathbf{p} = y\hat{a}_2 + z\hat{a}_3$ on the cross-section of the undeformed blade at a distance $\mathbf{r}^0 = (r + x)\hat{i}_1$ from the center of the hub (refer Fig. 1). After deformation of the blade, the point $\mathbf{p}$ moves to $\mathbf{p}^*$ whose location on cross-section

of deformed blade is $\mathbf{p}^* = y\hat{b}_2 + z\hat{b}_3$. The coordinates of a point on the cross-section remain the same because of the assumption that the shape of the cross-section remains intact after deformation. The elastic displacements of the blade are described in terms of three translation motions, $\mathbf{u} = u_k\hat{a}_k$ and corresponding three rigid body rotations of the cross-section, θ_k about $\hat{a}_k$, respectively. Thus, six time-dependent elastic deformation variables describe the motion of the blade. It is possible to express the deformation of the body either using Cartesian displacement variables, (u_k), or non-Cartesian deformation variables, $(s,\ u_k,\ k = 2,3)$, where s is a stretch variable. The displacement along the span of the blade, u_1, is commonly referred to as the *axial-motion*. u_2 and u_3 are transverse motions in the chord and the normal direction, respectively. In the literature dealing with rotating blade dynamics, u_2 and u_3 are most commonly referred to as the *chord-wise* and *flap-wise* motion, respectively. Now, the position vectors of $\mathbf{p}$ and $\mathbf{p}^*$ in the inertial reference frame can be written as follows

$$\begin{aligned}\mathbf{r_p} &= \mathbf{r^0} + \mathbf{R^0 p},\\ \mathbf{r_{p^*}} &= \mathbf{r^0} + \mathbf{R^0}(\mathbf{u} + \mathbf{u_g} + \mathbf{Rp}),\end{aligned} \tag{1}$$

where,

$$\{\mathrm{r}^0\} = \begin{pmatrix} r+x \\ 0 \\ 0 \end{pmatrix}, \quad [R^0] = \begin{bmatrix} c_\theta & -s_\theta & 0 \\ s_\theta & c_\theta & 0 \\ 0 & 0 & 1 \end{bmatrix}, \quad \{\mathrm{p}\} = \begin{pmatrix} 0 \\ y \\ z \end{pmatrix}, \quad \{\mathrm{u_g}\} = \begin{pmatrix} u_s \\ 0 \\ 0 \end{pmatrix} \quad \text{and} \quad \{\mathrm{u}\} = \begin{pmatrix} u_1 \\ u_2 \\ u_3 \end{pmatrix}. \tag{2}$$

In which u_s indicates the foreshortening effect, the longitudinal shrinkage of the elastic axis caused by the transverse motion. It is discussed in detail in the subsequent section. Here, $c_\theta = \cos\theta$, $s_\theta = \sin\theta$ and $\dot{\theta} = \Omega$. $\mathbf{R^0}$ is the rotational transformation matrix from the body reference frame, $\hat{\mathbf{a}}$, to the inertial reference frame $\hat{\mathbf{i}}$ so that $\hat{\mathbf{a}} = \mathbf{R^0}\hat{\mathbf{i}}$. The transformation matrix, $\mathbf{R}$, represents the transformation from the frame, $\hat{\mathbf{b}}$, to the frame, $\hat{\mathbf{a}}$, such that $\hat{\mathbf{b}} = \mathbf{R}\hat{\mathbf{a}}$. There are various representations of the transformation (rotation) matrix in the literature, the details of which can be found in standard reference books on multibody dynamics [44–46]. For instance, the matrix representing the rigid body rotation can be deduced in terms of the three Euler angles as shown in Fig. 2 [47]

$$\hat{\mathbf{b}} = \mathbf{R}\hat{\mathbf{a}}, \ \text{where,}\ [R] = \begin{bmatrix} c_2c_3 & c_2s_3 & -s_2 \\ s_1s_2c_3 - c_1s_3 & c_1c_3 + s_1s_2s_3 & s_1c_2 \\ s_1s_3 + c_1s_2c_3 & c_1s_2s_3 - s_1c_3 & c_1c_2 \end{bmatrix}. \tag{3}$$

Where, $c_k = \cos\theta_k$ and $s_k = \sin\theta_k$. For a non-shearable blade, the rotation matrix can be expressed in terms of the translation elastic displacement variables using the following relations [47],

$$c_2 = \frac{\sqrt{\left(1+u_1'\right)^2 + u_2'^2}}{1+e}, \quad s_2 = \frac{-u_3'}{1+e}, \quad c_3 = \frac{1+u_1'}{\sqrt{\left(1+u_1'\right)^2 + u_2'^2}}, \quad s_3 = \frac{u_2'}{\sqrt{\left(1+u_1'\right)^2 + u_2'^2}} \tag{4}$$

$$\text{where,} \quad e = \sqrt{\left(1+u_1'\right)^2 + u_2'^2 + u_3'^2} - 1.$$

and $()'$ indicates the derivative with respect to the spatial coordinate x. Another widely used method to represent the rigid body rotation is Rodrigues' rotation formula [28,46]. According to Euler's theorem on rotations, any arbitrary rotation of a rigid body can be viewed as a single rotation of magnitude α about a unit vector, $\hat{\mathbf{n}}$. This implies that four parameters are necessary to describe any rotational motion: (1) the three measure numbers of a unit vector, $\hat{n}_i$, along the line about which the rotation occurs, and (2) the magnitude of the rotation α. It can be further shown that with a normality constraint applied to the three components of a unit vector, the number of parameters necessary to describe any rotational motion reduces to three. Euler's theorem on rotations leads to a compact expression for the rotation tensor as given below [28,46]

$$\hat{\mathbf{b}} = \hat{\mathbf{a}} + (\sin\alpha)\tilde{\mathbf{n}}\hat{\mathbf{a}} + (1-\cos\alpha)(\tilde{\mathbf{n}}\tilde{\mathbf{n}})\hat{\mathbf{a}} = \overline{\mathbf{R}}(\alpha)\hat{\mathbf{a}}, \ \text{where,} \tag{5a}$$

$$\overline{\mathbf{R}}(\alpha) = \mathbf{I} + (\sin\alpha)\tilde{\mathbf{n}} + (1-\cos\alpha)\tilde{\mathbf{n}}\tilde{\mathbf{n}} \tag{5b}$$

$\overline{\mathbf{R}}$ and $\tilde{\mathbf{n}}$ are the rotation matrix and the cross product operator of a vector $\hat{\mathbf{n}}$, respectively. $\mathbf{I}$ is a identity matrix. This is known as Rodrigues' rotation formula. The formula is useful as a single rotation angle represents three-dimensional rigid body rotation. It is evident that a coordinate system after blade deformation can be brought to the coordinate system before blade deformation by a single rotation of magnitude α about an axis whose unit vector is $\hat{\mathbf{n}}$. This fundamental result expresses the rotation matrix in terms of a unit vector $\hat{\mathbf{n}}$ and a rotation of magnitude α about the unit vector. Pai [45] derives the expression for rotation matrix in terms of translation displacement variable and adopted for a fully consistent linearized model for vibration analysis of rotating beams in the framework of geometrically exact theory [48]. The rotation matrix is given by

$$[\bar{R}(\alpha)] = \begin{bmatrix} 1 & 0 & 0 \\ 0 & \cos\theta_1 & \sin\theta_1 \\ 0 & -\sin\theta_1 & \cos\theta_1 \end{bmatrix} \begin{bmatrix} R_{11} & R_{12} & R_{13} \\ -R_{12} & R_{11} + R_{13}^2/\left(1+R_{11}\right) & -R_{12}R_{13}/\left(1+R_{11}\right) \\ -R_{13} & -R_{12}R_{13}/\left(1+R_{11}\right) & R_{11} + R_{12}^2/\left(1+R_{11}\right) \end{bmatrix}, \tag{6}$$

where, θ_1 is the torsion motion, $R_{11} = \dfrac{1+u_1'}{1+e}$, $R_{12} = \dfrac{u_2'}{1+e}$ and $R_{13} = \dfrac{u_3'}{1+e}$. The rotation matrix $\overline{\mathbf{R}}$ is indeterminate when $R_{11} = -1$, which corresponds to $\alpha = 180^0$ and $R_{12} = R_{13} = 0$ [45]. To avoid the singularity of the rotation matrix that describes the rotation from $\hat{\mathbf{b}}$ frame to $\hat{\mathbf{a}}$ frame, four Euler parameters (referred to as quaternions) are used, which are identified as $e_0 = \cos(\alpha/2)$ and $e_i = \hat{n}_i \sin(\alpha/2)$. Now the rotation matrix in terms of quaternions is given by [28]

$$\overline{\mathbf{R}}(\alpha) = \left(1 - 2\mathbf{e}^{\mathrm{T}}\mathbf{e}\right)\mathbf{I} + 2\left(\mathbf{e}\mathbf{e}^{\mathrm{T}} - e_0\tilde{\mathbf{e}}\right) \tag{7}$$

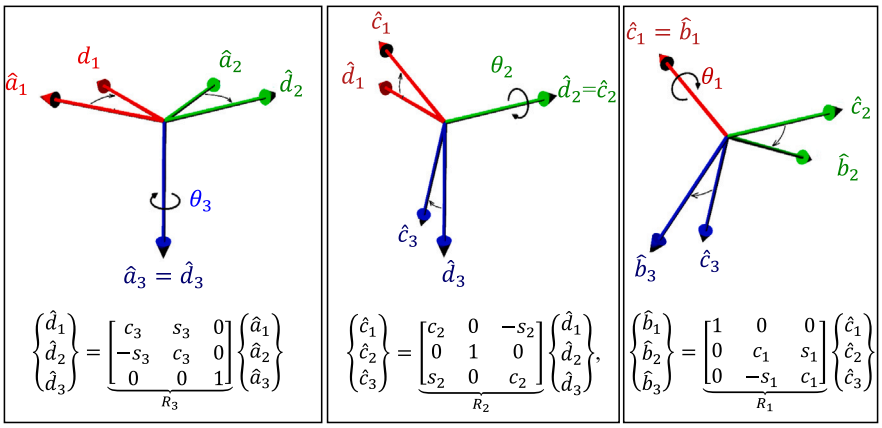

Fig. 2. Euler angles for 3-2-1 convention and the rotational matrix.

The four Euler parameters satisfy a normality constraint of the form $\mathbf{e}^{\mathrm{T}}\mathbf{e}+e_0^2=1$ and using this constraint, the number of parameters is reduced to three as given by $g_i = 2e_i/e_0 = 2\hat{n}_i\tan(\alpha/2)$. These three parameters are called Euler–Rodrigues parameters. The rotation matrix in terms of Euler–Rodrigues parameters is given by [28]

$$\overline{\mathbf{R}}(\alpha) = \frac{\left(1-\frac{1}{4}\mathbf{g}^{\mathrm{T}}\mathbf{g}\right)\mathbf{I}+\frac{1}{2}\mathbf{g}\mathbf{g}^{\mathrm{T}}-\tilde{\mathbf{g}}}{1+\frac{1}{4}\mathbf{g}^{\mathrm{T}}\mathbf{g}} \tag{8}$$

Rodrigues parameters increase the non-singularity range, and such a formulation is very convenient for analytical purposes. Now the position vector of an arbitrary point on the cross-section of the rotating blade is known. Further, the displacement field and velocity of the arbitrary point are derived and subsequently, the expressions for kinetic and strain energies are derived in the following section.

2.1. Kinetic energy

The velocity can be calculated using Eq. (1). Revisiting the position vector, it can be expressed as

$$\mathbf{r}_{\mathbf{p}^*} = (\mathbf{r^0}+\mathbf{R^0}\bar{\mathbf{u}})\hat{\mathbf{i}}. \tag{9}$$

Where, $\mathbf{r^0}$ is viewed as the position vector of the body reference frame, $\hat{\mathbf{a}}$ and $\bar{\mathbf{u}} = \mathbf{u}+\mathbf{u_g}+\mathbf{Rp}$ is the position vector of the arbitrary point on the deformed blade with respect to the body reference frame. This means the motion of the body is expressed as the motion of its body reference frame plus the motion of the material points on the body with respect to its body reference frame. Such representation is known as Floating Frame of Ref. [49]. The definition of $\bar{\mathbf{u}}$ consists of the longitudinal displacement due to the axial elastic motion of the points on the elastic axis of the beam, $\mathbf{u}$, the longitudinal displacement of the point on the elastic axis caused by the transverse deflection of the beam, $\mathbf{u_g}$ and the displacement associated with rotation of the plane section, $\mathbf{Rp}$, which equals zero on the neutral axis [50,51]. The velocity of the point $\mathbf{p}^*$ is given by the derivative of the position vector

$$\mathbf{v_p} = \mathbf{R^0}\dot{\bar{\mathbf{u}}}+\dot{\mathbf{R}}^{\mathbf{0}}\bar{\mathbf{u}}. \tag{10}$$

Where, $\dot{()}$ indicates the derivation with respect to time. The time derivative of any rotational matrix is given by $\dot{\mathbf{R}} = \boldsymbol{\omega}\times\mathbf{R} = \tilde{\boldsymbol{\omega}}\mathbf{R}$, where, $\boldsymbol{\omega}$ is the angular velocity vector with its components ω_i and $\tilde{\boldsymbol{\omega}}$ is the CPO of $\boldsymbol{\omega}$. The expression for components of angular velocity is given by $\omega_1 = \dot{R}_{2i}R_{3i}$, $\omega_2 = -\dot{R}_{1i}R_{3i}$ and $\omega_3 = \dot{R}_{1i}R_{2i}$, where, R_{ij} are elements of matrix $\mathbf{R}$ [45]. The second term of Eq. (10) which involves derivative of the rotation matrix is given by [49,52]

$$\mathbf{R^0}\dot{\bar{\mathbf{u}}} = \mathbf{R^0}(\dot{\boldsymbol{\Omega}\times\bar{\mathbf{u}}}) = -\mathbf{R^0}\tilde{\bar{\mathbf{u}}}\boldsymbol{\Omega}$$

Where the angular velocity vector, $\boldsymbol{\Omega}$, is given by $\{\Omega\} = \begin{pmatrix}0 & 0 & \Omega\end{pmatrix}^T$. $\tilde{\bar{\mathbf{u}}}$ is the cross product operator of the vector $\bar{\mathbf{u}}$. The velocity of the point is obtained as

$$\mathbf{v_p} = \mathbf{R^0}\dot{\bar{\mathbf{u}}}+\mathbf{B}\boldsymbol{\Omega} = \begin{bmatrix}\mathbf{R^0} & \mathbf{B}\end{bmatrix}\begin{bmatrix}\dot{\bar{\mathbf{u}}}\\ \boldsymbol{\Omega}\end{bmatrix}, \quad \text{where,} \quad \mathbf{B} = -\mathbf{R^0}\tilde{\bar{\mathbf{u}}}. \tag{11}$$

One can write the velocity vector as

$$\mathbf{v_p} = \mathcal{L}\mathcal{Q}, \quad \mathcal{L} = \begin{pmatrix}\mathbf{R^0} & \mathbf{B}\end{pmatrix} \quad \text{and} \quad \mathcal{Q} = \begin{pmatrix}\dot{\bar{\mathbf{u}}} & \boldsymbol{\Omega}\end{pmatrix}^T. \tag{12}$$

Table 1
Definitions of strain tensor [53] and expression of different axial strain for Euler–Bernoulli beam.

Strain tensor	Generalized expression	Euler–Bernoulli beam
Green–Lagrange (large deformation and large finite strain)	$\check{e}_{ij} = \frac{1}{2}\left(\frac{\partial \mathcal{U}_i}{\partial x_j} + \frac{\partial \mathcal{U}_j}{\partial x_i}\right) + \frac{1}{2}\frac{\partial \mathcal{U}_k}{\partial x_i}\frac{\partial \mathcal{U}_k}{\partial x_j}$ $\{x_i\} = \{x, y, z\}$, $\{\mathcal{U}_i\} = \{u, v, w, \}$ and x_i are reference coordinates (un-deformed state)	$\check{e}_{xx} = \frac{\partial u}{\partial x} + \frac{1}{2}\left[\left(\frac{\partial u}{\partial x}\right)^2 + \left(\frac{\partial v}{\partial x}\right)^2 + \left(\frac{\partial w}{\partial x}\right)^2\right]$
Euler–Almansi (large deformation and large finite strain,)	$e_{ij} = \frac{1}{2}\left(\frac{\partial \mathcal{U}_i}{\partial x_j} + \frac{\partial \mathcal{U}_j}{\partial x_i}\right) - \frac{1}{2}\frac{\partial \mathcal{U}_k}{\partial x_i}\frac{\partial \mathcal{U}_k}{\partial x_j}$ $i, j, k = 1, 2, 3$ and x_i are current coordinates (deformed state)	$e_{xx} = \frac{\partial u}{\partial x} - \frac{1}{2}\left[\left(\frac{\partial u}{\partial x}\right)^2 + \left(\frac{\partial v}{\partial x}\right)^2 + \left(\frac{\partial w}{\partial x}\right)^2\right]$
von Kármán (large deformation and small strain)	$\epsilon_{ij} = \frac{1}{2}\left(\frac{\partial \mathcal{U}_i}{\partial x_j} + \frac{\partial \mathcal{U}_j}{\partial x_i}\right) + \frac{1}{2}\frac{\partial \mathcal{U}_k}{\partial x_i}\frac{\partial \mathcal{U}_k}{\partial x_j}$ $i, j = 1, 2, 3$, $k = 2, 3$ and x_i are reference coordinates	$\epsilon_{xx} = \frac{\partial u}{\partial x} + \frac{1}{2}\left[\left(\frac{\partial v}{\partial x}\right)^2 + \left(\frac{\partial w}{\partial x}\right)^2\right]$
Cauchy (small deformation and small strain)	$\check{\epsilon}_{ij} = \frac{1}{2}\left(\frac{\partial \mathcal{U}_i}{\partial x_j} + \frac{\partial \mathcal{U}_j}{\partial x_i}\right)$ $i, j = 1, 2, 3$	$\check{\epsilon}_{xx} = \frac{\partial u}{\partial x}$

Where, $\boldsymbol{Q}$ is the total vector of generalized velocities of the blade and $\boldsymbol{\mathcal{L}}$ is the matrix. The expression for kinetic energy is given by

$$\mathrm{T} = \frac{1}{2}\int_L \int_A \rho(\mathbf{v_p^T v_p}) dA dx = \frac{1}{2}\boldsymbol{Q}^T \boldsymbol{\mathcal{M}} \boldsymbol{Q}. \tag{13}$$

Where, ρ, A and L are the density, cross-sectional area and length of the beam, respectively, and

$$\boldsymbol{\mathcal{M}} = \int_L \int_A \rho(\boldsymbol{\mathcal{L}}^T \boldsymbol{\mathcal{L}}) dA dx = \int_L \int_A \rho \begin{bmatrix} \mathbf{I} & \mathbf{R^{0^T} B} \\ Sym & \mathbf{B^T B} \end{bmatrix} dA dx = \int_L \rho \begin{bmatrix} \bar{\mathbf{M}} & \bar{\mathbf{G}} \\ Sym & \bar{\mathbf{K}}_s \end{bmatrix} dx \tag{14}$$

is the symmetric inertial matrix. Here, $\bar{\mathbf{M}}$ is inertial or mass matrix, $\bar{\mathbf{G}}$ is a Gyroscopic coupling matrix and $\bar{\mathbf{K}}_s$ is associated with rotation effect.

2.2. Strain energy

The displacement field, deformation gradient tensor and strain tensor are required to derive the expression for strain energy. The displacement field is given by $\mathbf{r_{p*}} - \mathbf{r_p}$ and can be expressed from Eq. (1) as

$$\mathcal{U} = \mathbf{r_{p*}} - \mathbf{r_p} = \mathbf{u} + \mathbf{u_g} + (\mathbf{R} - \mathbf{I})\mathbf{p} \tag{15}$$

The deformation gradient tensor $\mathbf{F}$ is expressed in terms of the displacement field as follows

$$\mathbf{F} = \mathbf{I} + \nabla \mathcal{U} \tag{16}$$

Where, $\nabla \mathcal{U} = \frac{\partial \mathcal{U}_i}{\partial x_j}$ is the tensor gradient of $\mathbf{u}$. The strain tensor is defined as the change in the squared lengths that occurs as a body deforms from the reference to the current configuration. Based on whether the change in the squared lengths is expressed relative to the original length or deformed (current) length, the strain field is named as either *Green–Lagrange strain tensor* or *Euler strain tensor*. These strain tensors are highly nonlinear and are used for the beam's large strain and large deformation analysis. The nonlinear part of the strain is insignificant for small strain and small deformation problems; hence it can be ignored. In such cases, the linear part of the Green–Lagrange strain tensor, known as *Cauchy strain tensor*, is only considered for the analysis. However, for a small strain and moderately large rotations $(10^0 - 15^0)$ of the beam, the longitudinal displacement is often a small quantity. Hence, the nonlinear terms due to longitudinal displacement and its gradient can be ignored from the Green–Lagrange strain tensor [53]. However, the gradient of the transverse displacements, which denotes the rotation of a line perpendicular to the beam axis, is not small and should be retained. The resulting strain tensor is nonlinear in that only squares of the normal plane rotations are included while neglecting the squares of the in-plane displacement terms. This strain tensor is called the *von Kármán strain tensor*. The different strain measures are summarized in Table 1.

With a continuum mechanics approach, the work done by elastic forces, δU, can be defined as [54]

$$\delta U = \int_V \mathbf{S}\, \delta \check{\mathbf{e}}\, \mathrm{d}V \tag{17}$$

where $\mathbf{S}$ is the second Piola–Kirchhoff stress tensor, $\check{\mathbf{e}}$ is the Green–Lagrange strain tensor, and V is the volume of the reference element. For the simplest case of a homogeneous isotropic elastic material – St. Venant–Kirchhoff material model – the second Piola–Kirchhoff stress tensor is linear with respect to the Green strain tensor. The relation between the stress tensor and strain tensor is given by $\mathbf{S} = \mathbf{E}\check{\mathbf{e}}$, where, $\mathbf{E}$ is the matrix of the elastic constants of the material [55,56]. In the case of a structural mechanics formulation based on the Bernoulli–Euler beam theory, the virtual work done by elastic forces can be defined as [54]

$$U = \int_V \check{\mathbf{e}}^{\mathbf{T}} \mathbf{E} \check{\mathbf{e}}\, \mathrm{d}V \tag{18}$$

Various geometrical stiffening models which employ different nonlinear strain measures listed in Table 1 for deriving the strain energy expression are presented in Section 3. For certain applications, such as helicopter or wind turbine blades, the deformation

of the blade can be significant due to its large slender geometry. In such applications, the strain can be small, but employing the linear strain measure can lead to inaccurate results. This is because the nonlinear part of the strain contains rigid-body rotations and local strains. It is required to decompose a rigid-body rotation part and a pure strain part and then ignore the nonlinear part associated with pure strain. One of the ways to achieve this is by polar decomposition of the deformation gradient, and the process of linearization with respect to pure strain is called consistent linearization. A brief detail of consistent linearization is presented in the following section.

2.3. Consistent linearization

The Green–Lagrange (GL) tensor $\check{\mathbf{e}}$ is given by

$$\check{\mathbf{e}} = \frac{1}{2}(\mathbf{F}^{\mathbf{T}}\mathbf{F} - \mathbf{I}) = \frac{1}{2}(\nabla\mathcal{U} + \nabla^{T}\mathcal{U} + \nabla^{T}\mathcal{U}\nabla\mathcal{U}). \tag{19}$$

For small strain and small deformation problems, the direct linearization assumes the rotation angle is small and then uses linear strain–displacement relation. Using the approximation $c_i = 1$ and $s_i = \theta_i$, the linear displacement field without foreshortening effect, $\mathbf{u}_g$, can be written as

$$\mathcal{U} = \begin{Bmatrix} u_1 \\ u_2 \\ u_3 \end{Bmatrix} + \begin{bmatrix} 0 & \theta_3 & -\theta_2 \\ -\theta_3 & 0 & \theta_1 \\ \theta_2 & -\theta_1 & 0 \end{bmatrix} \begin{Bmatrix} 0 \\ y \\ z \end{Bmatrix} \tag{20}$$

Such an approximation is suitable for small deformation problems and is adopted in most studies dealing with the linear analysis of rotating blades. For large deformation and small strain problems, a differential beam element can be subjected to a rigid-body motion, which can be large but minimally deformed. For such problems, we tend to ignore the nonlinear part of the Green–Lagrange strain tensor, $\nabla^{\mathbf{T}}\mathcal{U}\nabla\mathcal{U}$. However, the nonlinear part of the Green–Lagrange strain tensor represents both rigid-body rotations and local strains in a mixed manner. Linear approximation of the Green–Lagrange strain tensor can lead to inaccurate results [23]. For such problems, consistent linearization is performed in which the nonlinear term, $\nabla^{\mathbf{T}}\mathcal{U}\nabla\mathcal{U}$, is split into a rigid-body rotation part and a pure strain part and then linearizes the strain–displacement relation. This is not the only procedure for consistent linearization. Several other ways exist, such as linearization of the deformation gradient, linearization of the material strain matrix, linearization at an undeformed reference state and linearization of the determinant of the deformation gradient as discussed in [57]. The pseudo-polar decomposition of the deformation gradient can be given as $\mathbf{F} = \mathbf{R}(\mathbf{I} + \check{\mathcal{U}})$, where, $\mathbf{R}$ is the rotation tensor associated with the cross-section rotation as given in Eq. (3) and $\check{\mathcal{U}}$ is a stretch tensor, which corresponds to the part of the deformation gradient without the rigid-body displacement. Now, Green–Lagrange strain tensor takes a form $\check{\mathbf{e}} = \frac{1}{2}(\mathbf{F}^{\mathrm{T}}\mathbf{F} - \mathbf{I}) = \frac{1}{2}(\check{\mathcal{U}} + \check{\mathcal{U}}^{\mathrm{T}} + \check{\mathcal{U}}^{\mathrm{T}}\check{\mathcal{U}})$. For small strains problem, it is possible to neglect $\check{\mathcal{U}}^{\mathrm{T}}\check{\mathcal{U}}$ as it does not contain the rigid-body rotation [23].

2.4. Equations of motion

The equations of motion are derived based on energy or force-balance methods. Energy methods have some advantages over force-balance methods. The scalar quantity energy is typically easier to calculate than the vector quantity force. For rotating coordinate systems and/or systems with nonlinearities, the direct equilibration of all forces acting on the system is difficult as the decision of which forces are relevant and how they relate to the system state may take some discussion. With energy methods, the efforts spent setting up equations of motion are primarily on performing trivial mathematical operations, the correctness of which may be easily traced [58]. For obvious reasons, most rotating beam dynamics literature adopts the energy method, mostly either Lagrange's Equations or Hamilton's Principle. To apply the energy method, the most fundamental quantity in the mathematical analysis of mechanical problems, Lagrangian (L $= T - U$), is defined.

Lagrange's Equations are often a popular choice to set up the equation of motion for a rotating beam problem. However, Lagrange's equations apply to systems with finite degrees of freedom. Therefore, the continuous displacement variables in the kinetic and potential energies are expressed in terms of finite number generalized coordinates and generalized velocities. This is achieved by writing any continuous displacement variables, (w), in terms of a series of functions with many terms as

$$w(x,t) = \sum_{j=1}^{N_t} q_j(t)\phi_j(x), \quad j = 1, 2 \ldots Nt, \tag{21}$$

where, $q_j(t)$ are a set of time-dependent unknown generalized coordinates that uniquely define the state of the system and $\phi_j(x)$ are known space-dependent basis functions. The basis functions are a set of functions that satisfy the following criteria: It must be linearly independent, continuous and differentiable up to the order of the highest spatial derivative in the Lagrangian. It must also satisfy all or at least part of the boundary conditions. N_t is degrees of freedom. Then, the system of N_t number ordinary differential equations is derived using Lagrange's equations which are expressed as

$$\frac{d}{dt}\left(\frac{\partial \mathrm{L}}{\partial \dot{q}_j}\right) - \frac{\partial \mathrm{L}}{\partial q_j} = Q_j, \quad j = 1, 2 \ldots N_t, \tag{22}$$

where, Q_j are called the generalized forces representing the effects of all non-conservative forces in the system and L is the Lagrangian. This approximate technique is known as the Ritz method, which is applied to Lagrange's equations to derive the system of ordinary differential equations.

Alternatively, Hamilton's principle, which applies to a system with infinitely many degrees of freedom, is used to derive the partial differential equations. By Hamilton's principle [58],

$$\delta H = 0, \quad H \equiv \int_{t_1}^{t_2} L dt, \tag{23}$$

where, H defines the action integral and δH is the variation of H. t_1 and t_2 are arbitrary instants of time. Then, the system of ordinary differential equations is obtained by substituting Eq. (21) into the resulting partial differential equations. This procedure is called Galerkin's method, applied to partial differential equations derived using Hamilton's principle.

A set of basis functions used in the Ritz and Galerkin's method are admissible and comparison functions, respectively. The admissible functions are basis functions that satisfy at least all boundary conditions on displacement and rotation (geometric boundary conditions). Admissible functions do not need to satisfy the force and moment boundary conditions, but satisfying them may improve accuracy. On the other hand, comparison functions are the basis functions that satisfy the force and moment boundary conditions in addition to the geometrical boundary conditions. The following section discusses linear and nonlinear models of geometric stiffening in a rotating blade by approximating different terms in the strain–displacement relation.

3. Models of geometric/centrifugal stiffening

Different geometrical stiffening models are reviewed by approximating the rotating blade as an Euler–Bernoulli beam. In such an approximation, a straight line transverse to the axis of the un-deformed beam remains straight, inextensible, and normal to the mid-plane after deformation [53]. As discussed in the previous section, consistent linearization is performed to separate a rigid-body rotation and pure strain for large deformation and small strain problems. Then, the strain–displacement relation is linearized with respect to pure strain retaining the nonlinear curvature. The nonlinear curvature–displacement relation is obtained using the binomial expansion of rotation angle from Eq. (4). The resulting equations of motion are highly nonlinear. Previous authors adopted the modeling method to study the nonlinear dynamics of the rotating beam with additional inextensionality constraints resulting in *Inextensible Beam Model* [23,59–62].

For small rotation problems, rotation angles are approximated as $c_i = 1$ and $s_i = \theta_i$ and for such problems the linearized curvature–displacement relation, $\theta_2 = -u_3'$ and $\theta_3 = u_2'$, is valid. *prime* over the variable indicates the derivative with respect to x. Now, the displacement due to the cross-section rotation and foreshortening effect, respectively, are given by [50,63]

$$\mathbf{Rp} = \begin{pmatrix} -yu_2' - zu_3' \\ 0 \\ 0 \end{pmatrix} \quad \text{and} \quad \mathbf{u_g} = \begin{pmatrix} -\frac{1}{2}\int_0^x u_2'^2 d\zeta - \frac{1}{2}\int_0^x u_3'^2 d\zeta \\ 0 \\ 0 \end{pmatrix}. \tag{24}$$

where, zu_3' and yu_2' are the longitudinal displacements caused by the rotation of the cross-section. $\frac{1}{2}\int_0^x u_2'^2 d\zeta$ and $\frac{1}{2}\int_0^x u_3'^2 d\zeta$ are due to foreshortening effect, the longitudinal displacements due to bending motion. In such cases, the displacement field, ($\mathcal{U}_i = \{u, v, w\}$) of a non-shearable beam without torsional motion is given by (from Eq. (15))

$$\mathcal{U} = \begin{pmatrix} u \\ v \\ w \end{pmatrix} = \begin{pmatrix} u_1 - yu_2' - zu_3' - \frac{1}{2}\int_0^x u_2'^2\, d\zeta - \frac{1}{2}\int_0^x u_3'^2\, d\zeta \\ u_2 \\ u_3 \end{pmatrix}, \tag{25}$$

The strain is derived by substituting the displacement Eq. (25) into an appropriate expression of strain listed in Table 1, which is in turn used in Eq. (18) to obtain the expression for the strain energy. The effect of higher order terms in the longitudinal displacement due to foreshortening is investigated by El-Absy and Shabana [50]. The authors developed four beam models to examine the effect of geometric stiffness. In the first model, called the Consistent Complete Model (CCM), the effect of $\mathbf{u_g}$ is included while formulating both the inertia and elastic forces. In the second model, called the Consistent Incomplete Model (CIM), the effect of $\mathbf{u_g}$ is neglected in formulating both the elastic and inertia forces. In the third model, called the First Inconsistent Model (FIM), the effect of $\mathbf{u_g}$ is included in formulating the elastic forces, but this effect is neglected when the inertia forces are formulated. In the fourth model, the Second Inconsistent Model (SIM), the effect of $\mathbf{u_g}$ is included in formulating the inertia forces, but this effect is neglected when the elastic forces are formulated. All four models are summarized in Table 2. It can be observed that the stiffness matrix becomes complicated with higher-order terms if the effect of u_g is ignored. However, including the effect of u_g leads to a linear stiffness matrix but a complicated mass matrix involving higher-order terms.

The normal strain can be obtained considering a non-linear strain–displacement relationship (von Kármán) using the displacement field (25) as

$$\epsilon_{xx} = u' + \frac{1}{2}\left(v'^2 + w'^2\right) = u_1' - yu_2'' - zu_3'' \tag{26}$$

It can be observed that the consideration of the longitudinal displacement caused by the transverse deflection, u_g, eliminates the nonlinear terms from the von Kármán strain. As a result, the strain energy expression takes a simple form. This strain energy expression leads to a constant stiffness matrix. Therefore, the stiffness matrix derived, including the foreshortening effect, is a constant stiffness matrix. On the other hand, if the longitudinal displacement caused by the transverse deflection, u_g, is ignored, the expression for strain takes the form

$$\epsilon_{xx} = u' + \frac{1}{2}\left(v'^2 + w'^2\right) = u_1' - yu_2'' - zu_3'' + \frac{1}{2}\left(u_2'^2 + u_3'^2\right), \tag{27}$$

Table 2
Different beam models developed to study the effect of geometric stiffness forces in a rotating beam by El-Absy and Shabana [50].

Model	Is $\mathbf{u}_g$ included in kinetic energy?	Is $\mathbf{u}_g$ included in strain energy?	Comments
CCM	Yes	Yes	Cumbersome mass matrix but simplified stiffness matrix. The nonlinear model is stable
CIM	No	No	The model is stable only if nonlinear strain measurement is used.
FIM	No	Yes	Linear model with constant mass and stiffness matrix which is unstable at high rotational speed
SIM	Yes	No	Stable model but elastically nonlinear due to elastic coupling between axial and bending displacement

Which is nonlinear; substituting it in the strain energy expression leads to the stiffness matrix with higher-order terms. Further, the mass matrix is linear if the axial displacement due to bending is ignored in the derivation of the kinetic energy. In such cases, the expression for kinetic energy for the Euler–Bernoulli beam is obtained using Eqs. (13) and (20) as

$$T = \rho A \int_0^L \left[\left(\dot{u}_1 - \Omega u_2 \right)^2 + \left(\dot{u}_2 + \Omega (r + x + u_1) \right)^2 + \dot{u}_3^2 \right] dx, \tag{28}$$

Nevertheless, when the effect of the axial displacement due to bending is considered, the kinetic energy expression consists of higher-order terms. In such cases, higher-order terms in the mass matrix lead to numerical complications. Note that the model which includes $\mathbf{u}_g$ in the derivation of kinetic energy is elastically non-linear, leading to the elastic coupling between the axial and bending displacements.

The numerical results of El-Absy and Shabana [50] for the rotating beam demonstrate that it is not necessary to include the effect of the foreshortening terms, u_g, in the inertia forces in order to obtain a stable solution for the rotating beam at higher values of angular velocity. If this effect is consistently neglected in both the inertia and elastic forces in a nonlinear elastic model, the dynamic solution of the rotating beam equation remains stable at high angular velocity values. Therefore, most of the studies consistently ignore the effect of the foreshortening and employ the nonlinear strain measure for ease of mathematical derivation and numerical implementation. In such a case, the displacement field takes the following form

$$\mathcal{U} = \begin{pmatrix} u \\ v \\ w \end{pmatrix} = \begin{pmatrix} u_1 - y u_2' - z u_3' \\ u_2 \\ u_3 \end{pmatrix}. \tag{29}$$

It is clear from the previous discussion that the geometrical stiffening models either include the foreshortening effect in the strain energy expression and employ linear strain–displacement relation or ignore the foreshortening effect in the strain energy expression by employing nonlinear strain–displacement relation. These modeling methods are identical and the following section reviews such nonlinear modeling methods, which employ different nonlinear measures listed in Table 1.

3.1. Nonlinear models

The current section presents the nonlinear models that ignore the foreshortening effect while deriving the kinetic and strain energy expression and adopting nonlinear strain measures. These are essentially consistent incomplete models (the second model in Table 2) in which the inertial mass matrix is simplified and the stiffness matrix becomes cumbersome based on the type of nonlinear strain measure employed [64,65]. Previous authors have proposed various nonlinear modeling methods for capturing the geometrical stiffening effect [7–9,64,66,67]. As a result of different approximations of the strain field, the geometrical stiffening term takes different forms such as linear, second order or third order function of elastic displacement [5,8,64]. The nonlinear geometrical stiffening models based on the Green–Lagrange strain measure and von Kármán strain measure are elaborated on in the following section. It can be noted that all these nonlinear models consist of nonlinear equations and nonlinear/linear boundary conditions. The source of the nonlinearity is the coupling between the axial and bending motion. In the coupling between elastic coordinates, the modeling method is generally stable and accurately captures the geometric stiffening.

3.1.1. Green–Lagrange strain tensor

Various authors considered the geometric stiffening effect by adopting the fully non-linear Green–Lagrange strain tensor. The expression of Green–Lagrange strain for an Euler–Bernoulli beam is obtained by substituting the displacement field Eq. (29) into axial strain field Eq. (19) (refer to the first row of Table 1) as

$$\breve{e}_{xx} = u' + \frac{1}{2}\left(\underline{u'^2} + v'^2 + w'^2 \right), \tag{30}$$

where, elastic displacements u, v and w are given in Eq. (29). The strain field given in Eq. (30) accounts for a quadratic term of longitudinal displacement (underlined term) which most studies on the rotating beam dynamics ignore. This term cause interaction between the axial and transverse displacements, which is evident in the strain energy expression. According to the theory of

continuum mechanics, the second Piola–Kirchhoff stress measurement corresponds to a nonlinear Green strain measurement. Therefore, the second Piola–Kirchhoff stress measurement should be used to obtain the strain energy of the beam. Saint-Venant–Kirchhoff material model gives the relation between the second Piola–Kirchhoff stress and fully nonlinear Green strain for Euler–Bernoulli beam as $S_{xx} = \bar{E}\breve{e}_{xx}$, where, $\bar{E} = \frac{E(1-\nu)}{(1+\nu)(1-2\nu)}$ the elastic constant of the material. E and ν represent Young's modulus and Poisson ratio of the beam material. Therefore, the expression for the strain energy given in Eq. (18) for a uniform Euler–Bernoulli beam with a symmetric cross-section made up of isotropic material takes the form

$$U = \frac{1}{2}\int_L\int_A \bar{E}\breve{e}_{xx}^2 dA dx = \frac{1}{2}\int_L\int_A \bar{E}\left[u'^2 + \left(\underline{u'^3} + \underline{u'v'^2} + \underline{u'w'^2}\right) + \frac{1}{4}\left(\underline{u'^4} + v'^4 + w'^4\right) + \frac{1}{2}\left(\underline{u'^2v'^2} + \underline{u'^2w'^2} + w'^2v'^2\right)\right] dA dx, \tag{31}$$

The underlined terms in Eq. (31) arise from the quadratic axial displacement (u'^2) in Eq. (30). Higher-order axial displacement terms are double underlined, whose influence can be insignificant at lower rotation speeds and can be ignored, considering that the axial displacement is quite small compared with transverse displacement. Nevertheless, the double-underlined terms can significantly affect results at a very high rotation speed, the magnitude of which depends on the centrifugal force [68]. Further, the single underlined terms also generated by retaining the quadratic axial displacement in Eq. (30) show the interaction between the axial and transverse displacements. This axial-bending coupled motion causes a reduction in structural stiffness. As a result, the beam exhibits the geometric stiffening and softening phenomenon for different rotation speeds [68]. Further, Zhao and Wu [63] considered the fully non-linear Green–Lagrange strain measure and the corresponding second Piola–Kirchhoff stress measure to investigate the effect of the quadratic term of longitudinal motion in normal strain expression. The geometric stiffening term corresponding to Green–Lagrange strain measure is a cubic function of elastic deformations. This form of geometric stiffening term is obtained by solving extremely complicated higher-order non-linear coupled axial-bending equations, which is numerically quite challenging as the axial mode is associated with a higher frequency than the bending mode. A study by Zhao and Wu [63] concluded that the second-order elastic force contributing from u'^2 in the Green–Lagrange strain tensor does not change the results significantly at a lower rotation speed. Therefore, most of the studies ignore the second-order elastic term [64].

3.1.2. Von kármán strain tensor

Considering the fact that the axial displacement is much smaller in magnitude compared to the bending displacement, the quadratic term, u'^2, can be ignored in the strain–displacement relation. In such cases, von Kármán strain, which is valid for small strains and moderately large rotations, can be employed. For an Euler–Bernoulli beam, the axial strain is obtained by substituting the displacement field Eq. (29) into von Kármán strain field [9,53],

$$\epsilon_{xx} = u' + \frac{1}{2}\left(v'^2 + w'^2\right) = \underbrace{u_1' - yu_2'' - zu_3''}_{\epsilon^L} + \frac{1}{2}\underbrace{\left(u_2'^2 + u_3'^2\right)}_{\epsilon^N}. \tag{32}$$

The expression for strain energy given in Eq. (18) for a beam with a symmetric cross-section takes the form

$$U = \frac{1}{2}\int \Big[\underbrace{EAu_1'^2 + EI_z u_2''^2 + EI_y u_3''^2}_{U^L} + \underbrace{EA\left(u_1'u_2'^2 + u_1'u_3'^2\right)}_{U^{LN}} + \frac{1}{4}\underbrace{EA\left(u_2'^4 + u_3'^4 + 2u_2'^2u_3'^2\right)}_{U^N}\Big] dx, \tag{33}$$

where, $I_y = \int z^2 dA$ and $I_z = \int y^2 dA$ are the second moments of area, U^L and U^N are the linear and nonlinear parts of the strain energy coming from explicitly linear (ϵ^L) and nonlinear (ϵ^N) parts of the strain, respectively. However, U^{LN} is the nonlinear part of the strain energy representing coupling between the axial and transverse motion coming from the interaction of ϵ^L and ϵ^N. Using the expression for strain energy in Eq. (33) and kinetic energy in Eq. (28), the equations of motion for constant rotation speed can be derived using Hamilton's principle Eq. (23) as

$$\rho A\left[\ddot{u}_1 - \Omega^2(r + x + u_1) - 2\Omega\dot{u}_2\right] - \left(F_G\right)' = 0 \tag{34a}$$

$$\rho A\left[\ddot{u}_2 - \Omega^2 u_2 + 2\Omega\dot{u}_2\right] - \left(F_G u_2'\right)' + EI_z u_2^{iv} = 0 \tag{34b}$$

$$\rho A\ddot{u}_3 - \left(F_G u_3'\right)' + EI_y u_3^{iv} = 0, \tag{34c}$$

and the associated boundary conditions are given by

$$\begin{aligned} &u_1,\ u_2,\ u_3\big|_{x=0} = 0, \quad u_2',\ u_3'\big|_{x=0} = 0, \\ &u_1' + \frac{1}{2}\left(u_2'^2 + u_3'^2\right),\ u_2'',\ u_3''\big|_{x=L} = 0 \quad \text{and} \quad u_2''',\ u_3'''\big|_{x=L} = 0. \end{aligned} \tag{35}$$

Where, F_G is the geometric stiffening force term. Based on the different approximations of the strain energy/strain field, the geometric stiffening force in the bending equations takes a different expression as summarized in Table 3.

The nonlinear term, U^N, which involves fourth-order terms in strain energy expression, leads to the third-order elastic force in the bending equations (refer to the first row of Table 3). The equations of motion derived without approximating strain energy Eq. (33) are not only nonlinear, but one of the boundary conditions is also nonlinear. The stiffness matrix appearing due to this nonlinear term, U^N, is fundamentally a quadratic function of the elastic deformations. Some of the authors considered this highly nonlinear model (including both nonlinear terms of strain energy, U^N and U^{LN}) for studying rotating-beam dynamics [63,64,69].

Table 3
Different nonlinear models for geometric stiffening of the rotating beam based on von Kármán strain tensor.

Sl. No.	Terms retained in Eq. (33)	Geometric stiffening term, F_G, in Eq. (34)	Comments	Ref.
1	U^L, U^{LN}, U^N	$EA\left[u_1' + \frac{1}{2}\left(u_2'^2 + u_3'^2\right)\right]$	Fully nonlinear equations and nonlinear boundary conditions. A second-order nonlinear stiffness matrix.	[7,64,66,69–74]
2	U^L and U^{LN}	$EA(u_1')$	Nonlinear equations of motion but linear boundary conditions. First order stiffness matrix	[70,75–79]
3	U^s Eq. (36)	$EA(s')$	Nonlinear equations of motion but linear boundary conditions. First order stiffness matrix	[7,24]
4	U^L	$EA(u_{1s})$ (u_{1s} is steady-state axial deformation)	Linear equations and boundary conditions. Constant stiffness matrix	[48,63,75,76,80]

Nevertheless, the solution procedure for such a nonlinear model is increasingly cumbersome and computationally expensive. This model is also computationally inefficient as it needs to consider high-frequency axial modes to evaluate stiffness matrices of bending modes and is more complicated due to the presence of a second-order nonlinear matrix [9]. Nonlinear boundary conditions add more complexity to the solution procedure as this model fails to converge when the mode superposition is applied [24]. Sharf [64] gives the detailed derivation of an explicit expression for the strain energy, and different nonlinear terms resulting from the nonlinear strain–displacement relations are identified. The performance study of the nonlinear formulation shows that the third-order elastic force arising from the axial-bending coupling plays a critical role in predicting the response of the beam structure. The results show that the nonlinear formulation possesses slow convergence characteristics.

Some studies ignored U^N and considered only the first nonlinear term, U^{LN}, of the strain energy expression to derive governing equations. The resulting equations of motion are still nonlinear, but the associated boundary conditions become linear. The elastic force in the bending equations is a quadratic function of the elastic deformation (refer to the second row of Table 3). The stiffness matrix appearing due to the first nonlinear term, U^{LN}, is fundamentally a linear function of the elastic displacement rather than a constant matrix. This approach was adopted by many authors and concluded that it gives reasonably accurate results for rotating beam dynamics [70,75–77]. The complexity in the implementation of modal analysis is reduced. With linear boundary conditions, convergence is proven to be better. In this model, a time-dependent axial force is a function of axial displacement. The solution procedure for this approach is still challenging due to axial-bending coupled motion.

In conclusion, to account for the geometric stiffening, the classical method uses the nonlinear strain–displacement relation resulting in nonlinear equations of motion [8]. The nonlinear modeling methods can accurately model the geometrical stiffening effect but are relatively cumbersome and computationally inefficient. The inefficiency of these models is attributed to the coupling of longitudinal and transverse modes, which are not of the same order. The longitudinal mode is one order of magnitude smaller and has a higher frequency relative to the transverse mode. To correctly represent the dynamics of the system, it is necessary to include a larger number of modes in computation [9]. To relax the complexity due to coupled axial-bending motion, a new dynamics model was proposed in which equations of motion are derived in terms of the new variable, stretch. The stretch-based nonlinear model is presented in the following section.

3.1.3. Stretch based nonlinear model

As mentioned in the introduction, the deformation of the blade can be expressed in terms of a non-Cartesian variable, stretch, which is measured using coordinates after deformation. The detailed derivation of the relation between stretch and bending motions is given in Section 3.2.3. The stretch (s), axial, chord-wise and flap-wise displacement are related by

$$s = u_1 + h_2 + h_3, \quad \text{where,} \quad h_2 = \frac{1}{2}\int_0^x \left(\frac{\partial u_2}{\partial \zeta}\right)^2 d\zeta \quad \text{and} \quad h_3 = \frac{1}{2}\int_0^x \left(\frac{\partial u_3}{\partial \zeta}\right)^2 d\zeta.$$

The expression of the strain energy takes the form as

$$U^s = \frac{1}{2}\int (EAs'^2 + EI_z u_2''^2 + + EI_y u_3''^2) dx \tag{36}$$

It is observed that the strain energy is now free from the axial-bending coupling terms and takes the same form as in the linear formulation without nonlinear terms. Therefore, the stiffening effect does not appear now in the elastic forces. The strain energy expression is simplified, but the kinetic energy expression gets complicated as stiffening terms are translated into inertia forces. This is because the foreshortening effect is now introduced explicitly in the displacement field at the kinematic level through the stretch variable. This model is similar to the second inconsistent model (SIM) in Table 2 where the foreshortening term is included while deriving the kinetic energy but ignored in the strain energy. The equations of motion can be written as [24]

$$\rho A\left[\ddot{s} - \ddot{h}_2 - \ddot{h}_3 - 2\Omega\dot{u}_2 \ -\Omega^2\left(a + x + s - h_2 - h_3\right)\right] - F_G' = 0, \tag{37a}$$

$$\rho A\left[\ddot{u}_2 + 2\Omega\left(\dot{s} - \dot{h}_2 - \dot{h}_3\right) - \Omega^2 u_2\right] - (F_G u_2')' + EI_z u_2^{iv} = 0 \quad \text{and} \tag{37b}$$

$$\rho A\ddot{u}_3 - (F_G u_3')' + EI_y u_3^{iv} = 0, \tag{37c}$$

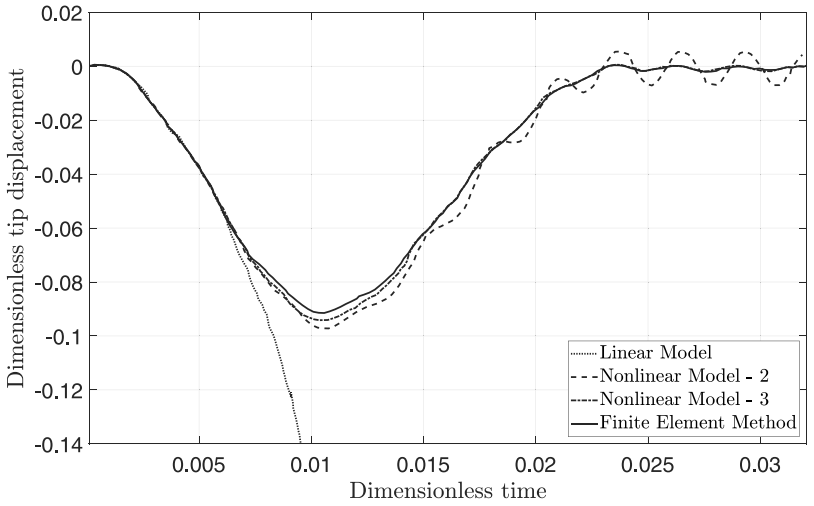

Fig. 3. The dimensionless tip displacement (w/L) of a spinning flexible beam at $\Omega = 6$ rad/s vs. dimensionless time $t\sqrt{E/\rho L^2}$ with properties of the beam E = 68.95 GPa, $\rho = 2766.67$ kg/m^3, L = 8 m, A = 7.3×10^{-5} m^2, I$_z$ = 8.218×10^{-9} m^4. Comparison of different nonlinear models: *Nonlinear Model-2*, *Nonlinear Model-3* and *Linear Model* indicate the modeling method 2, 3 and 4 mentioned in Table 3. *Finite Element Method* refers a non-incremental finite-element procedure [9].

where, $F_G = EAs'$. The associated boundary conditions are given by

$$\begin{aligned} &s,\ u_2,\ u_3\Big|_{x=0} = 0, \quad u_2',\ u_3'\Big|_{x=0} = 0, \\ &s',\ u_2'',\ u_3''\Big|_{x=L} = 0 \quad \text{and} \quad u_2''',\ u_3'''\Big|_{x=L} = 0. \end{aligned} \tag{38}$$

It can be noticed that the equations of motion given in Eq. (37) are nonlinear. However, the associated boundary conditions given in Eq. (38) become linear in the stretch-based formulation, which is derived without approximating the strain energy expression Eq. (33). Compassion study of the different nonlinear models is demonstrated using a benchmark problem, spinning flexible beam, for geometrically nonlinear formulations [9,64,67,81–83]. It involves a beam pinned at one of its ends which is allowed to rotate about the pinned end at an angular velocity, Ω. The results of the linear model and finite elements procedure are compared with two different nonlinear models for $\Omega = 6$ rad/s in Fig. 3 [9].*Linear Model* and *Nonlinear Model-2* (refer fourth and second row in Table 3) employ terms U^L and $(U^L + U^{LN})$, respectively, in the strain energy expression in Eq. (33). *Nonlinear Model-3* (refer third row in Table 3) is based on stretch variable given in Eq. (36) (Section 3.1.3). The *Finite Element Method* refers to the results obtained using a non-incremental finite-element procedure [84]. The linear model results without the effects of nonlinear geometric terms are divergent and inconsistent with the actual physical response. The results of *nonlinear model-2*, which is based on third-order terms in the strain energy (U^{LN} in Eq. (33)) are oscillatory. Also, the modeling method involves the product of derivatives of the axial displacement and the square of the derivatives of the transverse displacement. Therefore, many modes must be considered due to the coupling between the axial and transverse deformations. However, the results of *nonlinear model-3* agree with the results of the finite element procedure. The authors concluded from the results that nonlinear Model-3 based on the stretch variable is accurate and more efficient as it does not need to account for many axial modes. Kim and Chung [24] also compared these nonlinear models and concluded that the *nonlinear model-3* is more accurate than the other two nonlinear models given in the Table 3. The authors used the Galerkin method with the eigenfunctions of linear, stationary Euler–Bernoulli beam satisfying cantilevered boundary conditions for these nonlinear models. The assumed mode method applied to *nonlinear model-3* gives faster-converged solutions, whereas *nonlinear model-1* failed to give a converged solution. Applying the finite element method to *nonlinear model-1* may give a converged solution, but it requires considering many more degrees of freedom compared to the Galerkin method applied to *nonlinear model-3*. The subsequent section presents the linear modeling methods used for studying the rotating beam dynamics.

3.2. Linear models

It is clear from Fig. 3 that the results obtained for the linear formulation cannot account for the geometric stiffening effect. The tip deflection becomes too large as the simulation progresses. Considering Eq. (34b) without nonlinear and gyroscopic term

$$\begin{aligned} &\ddot{u}_2 - \Omega^2 u_2 + \frac{EI_z}{\rho A} u_2^{iv} = 0, \ \text{ using } \ u_2 = \phi_2(x) q_2(t), \\ &\ddot{q}_2 + (\omega^2 - \Omega^2) q_2 = 0, \end{aligned} \tag{39}$$

where, $\omega = \alpha^2\sqrt{\frac{EI}{\rho A}}$ are natural frequency and $\phi_2(x)$ and α are eigenfunction corresponding to the cantilever boundary condition and root of the characteristic equation of the cantilever beam, respectively. The equation indicates that the stiffness reduces with the

rotation speed. For ($\omega^2 < \Omega^2$), the stiffness can become negative, and the bending motion becomes unbounded, which is unrealistic. Also, ignoring the nonlinear term in Eq. (34c) means there is no rotation effect on the flap-wise bending motion. In reality, the rotation speed increases the flap-wise stiffness and, consequently, the natural frequency. It can be inferred that use of a geometrically linear beam theory results in equations of motion that predict a spurious loss of stiffness [11]. The inadmissible destabilization effects that are not present in the physical model exhibited by the formulation that adopts the linear strain–displacement relation were demonstrated by the previous authors [5,11,50]. The instability of the elastically linear models is believed to be due to the decoupling between the longitudinal and transverse displacements. When the coupling is neglected, the bending deformation of the beam does not cause any variation in the longitudinal displacement. Several authors proposed an alternate method to include the geometrical stiffening in the elastically linear models. El-Absy and Shabana [50] demonstrated that including the foreshortening effect in the expression of the inertia forces leads to a consistent model that automatically accounts for the stiffening effect. Another possible way to include the stiffening effect due to the rotation in the elastically linear models is by introducing the stiffening effect as a pre-stressed reference condition [2]. Berzeri and Shabana in [84] introduced a non-incremental finite element procedure called the absolute nodal coordinate formulation that employs global coordinates as nodal degrees of freedom to address the problem of centrifugal stiffening in the rotating beam. The following section elaborates on different approaches to include geometrical stiffening terms in linear models.

3.2.1. Constant centrifugal force

One of the straightforward ways to incorporate the stiffening effect in the linear analysis is to add the potential energy due to the rotation-induced centrifugal force to the expression of elastic potential energy [10,85]. The equations of motion derived by resorting to a time-independent centrifugal load are equivalent to those that govern the transverse vibrations of beams subject to an external axial force. In this approach, a linear Cauchy strain measurement is adopted. A time-independent axial force induced by the centrifugal force on the bending motion is obtained from the equation [86,87]

$$F_G = EAu_1' = \rho A \int_x^L \Omega^2(r+x)dx, \tag{40}$$

the solution of which is included directly in the strain energy. The equations of motion and associated boundary conditions obtained using the constant centrifugal force are linear. Various authors adopt this model [86,88–90]. The shortcoming of this approach is that the model produces unacceptable results for dynamic analysis of a rotating beam in the presence of the applied forces and for non-constant rotating speed [76]. Such a model gives inaccurate results at a relatively higher rotation speed.

3.2.2. Linearization around the solution of steady-state axial motion

When the nonlinear terms are ignored, the resulting model does not include the geometric stiffening effect. The previous authors linearized the equations of motion by coupling the equation governing the steady-state axial deformation with the transverse motion equation. A steady-state equilibrium equation is obtained from the axial deformation equation by ignoring the time-dependent part and its coupling with bending motion. The time-independent solution of the steady-state equilibrium equation, which represents the axial force $F_G = EAu_{1s}'$, is incorporated in the bending motion equation. Based on the strain–displacement relation adopted, the equation of steady-state axial deformation can be linear or nonlinear, as listed in Table 4. Most of the studies [76,91] used a linear steady-state equation of the form

$$\rho A\Omega^2(r+x) + EAu_{1s}'' = 0. \tag{41}$$

Interestingly, the axial force at a distance x computed by solving linear steady-state equilibrium Eq. (41) is identical to the centrifugal axial force obtained by Eq. (40). Therefore, the methods of computing axial force using static axial deformation equation or directly using constant centrifugal force in the elastic energy eventually are the same even though the approaches of these formulations are different from each other. As mentioned above, this simplified linear model produces inaccurate results at higher rotation speeds. Kim et al. [75] proposed a new model which adopts a linear steady-state equation with an additional term, u_{1s}. A new equation takes a form

$$\rho A\Omega^2(r+x+u_{1s}) + EAu_{1s}'' = 0. \tag{42}$$

This boundary-value problem is solved using the cantilever boundary conditions. The authors demonstrated that the results obtained using this model are accurate at a high rotation speed, as shown in Fig. 4. The natural frequencies computed using the two models do not exhibit significant differences in the low rotating speed range. However, the differences become prominent in the high rotating speed range. A similar study was conducted by Zhao and Wu [63] using different models of axial static equilibrium equation considering linear and nonlinear terms arising from the quadratic term of longitudinal deformation in strain–displacement relation. The nonlinear steady-state axial equilibrium equation was derived by Zhao and Wu [63]

$$\rho A\Omega^2(r+x+u_{1s}) + EA\left(u_{1s}'' + 3u_{1s}'u_{1s}'' + \frac{3}{2}u_{1s}'^2u_{1s}''\right) = 0.$$

The solution to this highly nonlinear equation is increasingly complicated with nonlinear terms. Therefore the authors have approximated the above nonlinear equation and arrived at three simpler models by ignoring different nonlinear terms, reducing to the form mentioned in Eq. (41), (42) and (44).

$$\rho A\Omega^2(x+u_{1s}) + EA(u_{1s}'' + 3u_{1s}'u_{1s}'') = 0 \tag{43}$$

Table 4
The geometric stiffening force arises from the longitudinal shrinkage caused by the transverse bending displacement (foreshortening effect). $F_G = EAu'_{1s}$ is stiffening force in Eq. (34) and u'_{1s} is a solution of equation governing steady-state axial deformation.

Model No.	Steady-state axial equation	Approximate solution and stiffening force, $F_G = EAu'_{1s}$	Ref.
	Green–Lagrange Strain tensor		
1	$\rho A\Omega^2(x+u_{1s}) + EA(u''_{1s} + 2\vartheta u'_{1s}u''_{1s}) = 0$	$u_{1s} = c_1(\frac{x}{2} - \frac{x^3}{6})$ and $u'_{1s} = c_1(\frac{1}{2} - \frac{x^2}{2})$	[48,92]
2	$\rho A\Omega^2 x + EA(u''_{1s} + 3u'_{1s}u''_{1s}) = 0$	$u_{1s} = -\frac{x}{3} + \frac{\gamma}{\sqrt{3}}\left[\frac{x}{2}\sqrt{f_s - x^2} + \frac{f_s}{2}\arcsin(\frac{x}{\sqrt{f_s}})\right]$ $u'_{1s} = -\frac{1}{3} + \frac{\gamma}{\sqrt{3}}\left[\sqrt{f_s - x^2}\right]$	[63]
	von Kármán Strain tensor		
3	$\rho A\Omega^2(r+x+u_{1s}) + EAu''_{1s} = 0$	$u_{1s} = \frac{r\gamma\cos\left(\gamma(1-x)\right)+\sin(\gamma x)}{\gamma\cos(\gamma)} - (r+x)$ $u'_{1s} = \frac{r\gamma\sin\left(\gamma(1-x)\right)+\cos(\gamma x)}{\cos(\gamma)} - 1$	[63,75,91,93,94]
4	$\rho A\Omega^2(r+x) + EAu''_{1s} = 0$	$u_{1s} = \gamma^2\left[\frac{r}{2}(2x - x^2) + \frac{1}{6}(3x - x^3)\right]$ $u'_{1s} = \gamma^2\left[r(1-x) + \frac{1}{2}(1-x^2)\right]$	[63,72,76,80,88,95–97]
	Centrifugal force		
	$\int_0^1 \gamma^2(r+x)dx$	$\gamma^2\left[r(1-x) + \frac{1}{2}(1-x^2)\right]$	[86,87,89,90,98–101]

$\gamma = \Omega\sqrt{\frac{\rho L^2}{E}}$, $f_s = \frac{1}{3\gamma^2} + 1$, $c_1 = \frac{\sqrt{1764 - 1428\gamma^2 + 3024\vartheta\gamma^2 + 289\gamma^4} - 42 + 17\gamma^2}{36\vartheta}$, ϑ– Coefficient of non-linearity,

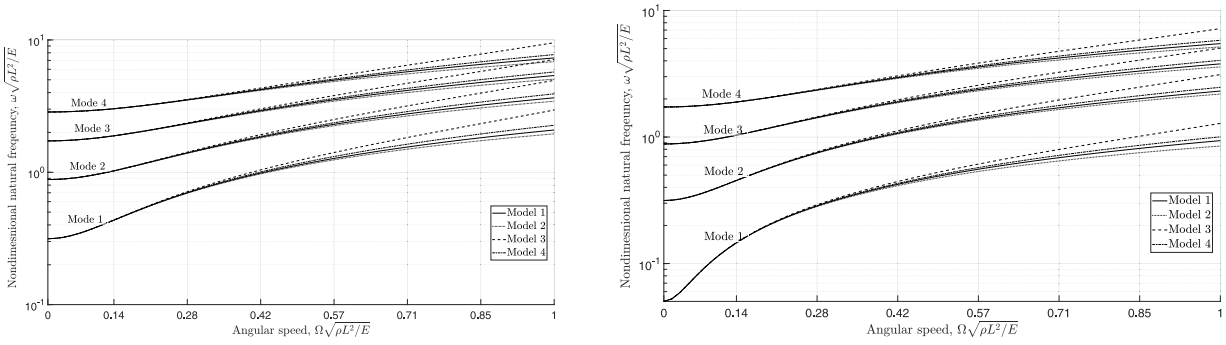

(a) The axial and chord-wise natural frequency (b) The flap-wise natural frequency

Fig. 4. The natural frequencies of Euler–Bernoulli beam obtained using four different linear modeling methods [75]. The geometric stiffening force, $F_G = EAu'_{1s}$, in Eq. (34) was calculated based on the solution of Eq. (41)–(44). The four linear models are listed in Table 4.

Invernizzi and Dozio [48] adopted the nonlinear model proposed by Hodges and Bless [92] of the form

$$\rho A\Omega^2(x+u_{1s}) + EA(u''_{1s} + 2\vartheta u'_{1s}u''_{1s}) = 0. \tag{44}$$

Where, ϑ is the coefficient of non-linearity, which depends upon the material and section geometry of the beam and must be determined experimentally. Invernizzi and Dozio compared the results of Kim's model (linear model Eq. (42)) with that of Hodge and Bless (Nonlinear model Eq. (44)) by computing the axial tip displacement and the axial root strain. The summary of different linear steady-state equilibrium equations ((41)–(44))and their solutions (steady-state axial displacement and strain) are summarized in Table 4.

Further, the comparison of the natural frequencies of the Euler–Bernoulli beam obtained by coupling the time-independent solution of four steady-state models Eqs. (41), (42),(43) and (44) with transverse motion equation are given in Fig. 4. The difference in the bending natural frequency is more at a higher rotation speed. Such a comparison between two models (41) and (42) is reported in the literature [75,94]

3.2.3. Hybrid deformation variable

As discussed in the previous section, the nonlinear formulations do not explicitly consider the foreshortening effect. On the other hand, the classical linear methods do not incorporate the geometric stiffening effect. Some linearized dynamics models consider the geometric stiffening effect through a constant axial force in bending equations. Still, such methods are inaccurate for dynamic modeling of the rotating beams at high rotation speed and under external excitation. A new formulation was developed that distinguishes between the longitudinal displacement due to the axial deformation and the longitudinal displacement caused by the transverse deflection of the beam (foreshortening) [7,8,102]. A new variable, namely stretches s, representing deformed longitudinal displacement (instead of undeformed in the previous model), was introduced. The relation between stretch and

transverse displacements is given by

$$s = u_1 + u_{fs}, \quad u_{fs} = \frac{1}{2}\int_0^x \left[\left(\frac{\partial u_2}{\partial \zeta}\right)^2 + \left(\frac{\partial u_3}{\partial \zeta}\right)^2\right] d\zeta. \tag{45}$$

Where, u_{fs} is an axial foreshortening displacement caused by the geometric non-linear coupling effect of the transverse displacements. This approach, which explicitly includes the foreshortening effect to incorporate the geometrical stiffening effect, was proposed by Kane et al. [5]. The authors proposed this formulation for the dynamics of an elastic body in which the axial displacement, as a dependent variable in the conventional methods, was replaced by a non-Cartesian *stretch deformation variable*, s. The authors described the stretch deformation in terms of linear axial deformation and first-order non-linear transverse deformation. Therefore, stretch is generally referred to as a hybrid or non-Cartesian variable. The derivative of the stretch

$$s' = u_1' + \frac{1}{2}u_2'^2 + \frac{1}{2}u'_3$$

is identical to the geometric stiffening force term, F_G, in Eq. (34) when fully nonlinear von Kármán strain field is adopted (Model-1 in Table 3). Hence, the dynamics model that uses the hybrid deformation variable is equivalent to the model that adopts second-order nonlinearity from the von Kármán strain field. The advantage is that the strain energy expression becomes linear and stiffness terms only include the constant elastic stiffness matrix and non-linear terms are moved to inertial, external and constraint forces [9]. Hence, contributing centrifugal stiffening terms arise pretty naturally from the kinetic energy expression instead of adding a constant centrifugal term [3]. Therefore, the resulting equation of motion is still non-linear, but associated boundary conditions are linear. The solution of such a model has better convergence and accuracy when the assumed mode method is applied as it is relatively easy to find the basis functions for linear boundary conditions [24,103]. This formulation includes the effect of all the geometric elastic nonlinearities on the bending displacement without requiring high-frequency axial modes due to the coupling between high-frequency axial and low-frequency bending modes. Also, the dynamic model based on the stretch variable is computationally efficient as a linear formulation [7]. Thomas et al. [23] derived the coupled non-linear equations of motion governing the flap-wise motion and the axial force $N = EA(u_1' + 0.5u_2'^2)$. The author derived equations of motion in terms of N instead of u_1. This model was compared with the inextensible model, which considers higher-order geometrical nonlinearities. The inextensible model was an extension to the rotating case of the elastica model proposed for non-rotating beams in [104–106]. The dynamic model proposed in [23] based on a new variable N, integration of which gives the longitudinal displacement in deformed condition (stretch) was proven to be efficient and accurate for computing modal characteristics.

The relation between the elastic deformation variable, u_k and the stretch deformation, s can be obtained. The strain energy and the kinetic energy are then expressed in terms of the stretch variable. Consider a differential element of length $d\eta$ on the neutral axis at a distance $x + u_1$ from the fixed end. The variable η varies from 0 to $x + u_1$. The change in the transverse deformations of the differential arc of the neutral axis is du_3 and du_3 as shown in Fig. 5. The differential length on the neutral axis of the deformed beam can be written as

$$ds = \sqrt{(d\eta)^2 + (du_2)^2 + (du_3)^2}.$$

The integration of the above equation with a limit from 0 to $(x + u_1)$ gives $x + S$, which the arc length from the fixed end of the beam to an arbitrary point p^* of the deformed beam. Since u_1 is explicitly involved in the limit of integration, the derivation of the equations of motion is complicated and the approach poses numerical and analytical challenges. To avoid the explicit dependence of the longitudinal displacement on the limit of integration, a new variable, $\zeta = \eta - u_1$, which varies from 0 to x, is introduced. At a fixed end of the beam, the axial deformation is zero (i.e, for $\eta = 0$, $u_1 = 0$ hence $\zeta = 0$). At $\eta = x + u_1$, it follows that $\zeta = x$. The differential arc length in terms of the new variable is given as

$$\begin{aligned} ds &= \sqrt{(d\zeta + du_1)^2 + (du_2)^2 + (du_3)^2} \\ &= \left[\left(d\zeta + \frac{\partial u_1}{\partial \zeta}d\zeta\right)^2 + \left(\frac{\partial u_2}{\partial \zeta}d\zeta\right)^2 + \left(\frac{\partial u_3}{\partial \zeta}d\zeta\right)^2\right]^{\frac{1}{2}}. \end{aligned} \tag{46}$$

The total length of the neutral axis after deformation is obtained by integrating Eq. (46) as

$$S = \int_0^x \left[\left(1 + \frac{\partial u_1}{\partial \zeta}\right)^2 + \left(\frac{\partial u_2}{\partial \zeta}\right)^2 + \left(\frac{\partial u_3}{\partial \zeta}\right)^2\right]^{\frac{1}{2}} d\zeta \tag{47}$$

Using binomial expansion, $\left(1 + \frac{\partial u_1}{\partial \zeta}\right)^2 \approx 1 + 2\frac{\partial u_1}{\partial \zeta}$, the arc length is given by

$$S = \int_0^x \left[1 + \left\{2\frac{\partial u_1}{\partial \zeta} + \left(\frac{\partial u_2}{\partial \zeta}\right)^2 + \left(\frac{\partial u_3}{\partial \zeta}\right)^2\right\}\right]^{\frac{1}{2}} d\zeta \tag{48}$$

Again expanding the terms in square bracket using $(1 + x)^{\frac{1}{2}} = 1 + \frac{x}{2} + \ldots$, the total length of the neutral axis which is equal to $S = x + s$, given as

$$x + s = x + u_1 + \frac{1}{2}\int_0^x \left[\left(\frac{\partial u_2}{\partial \zeta}\right)^2 + \left(\frac{\partial u_3}{\partial \zeta}\right)^2\right] \mathrm{d}\zeta. \tag{49}$$

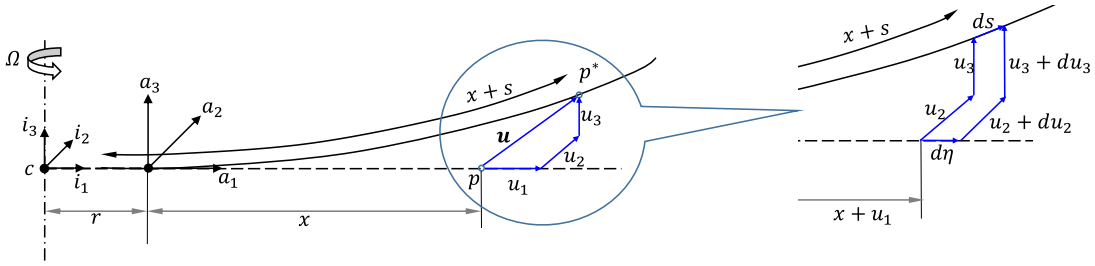

Fig. 5. Differential element on the neutral axis of a beam.

The relation between the elastic deformation variables and the stretch in the beam along the elastic axis is (refer Fig. 5)

$$s = u_1 + \frac{1}{2}\int_0^x \left(\frac{\partial u_2}{\partial \zeta}\right)^2 d\zeta + \frac{1}{2}\int_0^x \left(\frac{\partial u_3}{\partial \zeta}\right)^2 d\zeta. \tag{50}$$

Here, the longitudinal displacement after differentiating with respect to x gives

$$s' = u_1' + \frac{1}{2}u_2'^2 + \frac{1}{2}u_3'^2. \tag{51}$$

Now, the strain field given in (32) reduced to $\epsilon_{xx} = s' - yu_2'' - zu_3''$. The nonlinear terms vanished and the strain field is now linear. The strain energy expression is given in Eq. (18), now can be expressed in terms of stretch deformation as,

$$U = \frac{1}{2}\int (EAs'^2 + EI_z u_2''^2 + EI_y u_3''^2)dx \tag{52}$$

Though the strain energy expression becomes simple, the stretch variable adds more terms to the kinetic energy expression. The kinetic energy given in Eq. (28) becomes

$$\begin{aligned} T =& \rho A \int_0^L \left[\left(\dot{s} - \int_0^x u_2' \dot{u}_2 d\zeta - \int_0^x u_3' \dot{u}_3 d\zeta - \Omega u_2 \right)^2 + \right. \\ & \left. \left(\dot{u}_2 + \Omega\left(r + x + s - \int_0^x u_2'^2 d\zeta - \int_0^x u_3'^2 d\zeta \right) \right)^2 + \dot{u}_3^2 \right] dx \end{aligned} \tag{53}$$

The use of stretch variables enables non-linear terms of elastic force to move to inertial forces. As a result, the centrifugal stiffness matrix appears as an explicit function of the rotation speed. Choice of stretch, instead of axial deformation, to describe the kinematics of the deformed beam account that every transverse displacement gives rise to an axial displacement [5]. Up on expanding Eq. (53), we arrive at a linear term

$$\int \rho A\Omega^2 (r + x)\left[s - \frac{1}{2}\int_0^x \left(u_2'^2 + u_3'^2 \right) d\zeta \right] dx.$$

On integration by parts, it is possible to write it as

$$\int \rho A\Omega^2 \left((r + x)s - \frac{F_a}{2}\left[u_2'^2 + u_3'^2 \right] \right) dx, \tag{54}$$

where, $F_a = r(L - x) + \frac{1}{2}(L^2 - r^2)$. The form of the centrifugal forcing term is similar to that of the solution of Eq. (41).

Yoo et al. [107] demonstrated that the linear modeling method based on hybrid displacements (stretch) is accurate and computationally efficient. The method was proven to capture the motion-induced stiffness variations accurately and efficiently. Although linear strain measures were employed, this method was proved to be accurate for a structure subjected to an external torque and an external force [108]. Kim and Chung [24] demonstrated that the modeling method using the hybrid displacements is more accurate and has faster convergence characteristics when the modal analysis is used for the discretization of the nonlinear system. They compared their modeling method with the model constructed using the Cartesian variables. Yoo and Shin [96] adopted the method to investigate the dynamics of a rotating blade undergoing the three translation motions. Further, the method was successfully used for various problems like the rotating pre-twisted blade [6], rotating multi-layered composite blades [109], pre-twisted rotating Timoshenko blades [110], rotating double-tapered Timoshenko blades [111] and rotating wind turbine blade subjected gravitational force [112].

Another widely used method to include the geometrical stiffening in rotating beam is based on a non-incremental finite element procedure known as Absolute Nodal Coordinate Formulation [84,113,114]. As discussed, the floating frame of reference approach uses two sets of coordinates (reference coordinates described in global/inertial frames of reference and elastic coordinates described in the body or non-inertial frames of reference) to describe the dynamics of deformable bodies that undergo large reference displacements. The deformation of the body with respect to the body reference frame is defined using local coordinates, which

leads to a simple expression for the elastic forces. As a result of using local coordinates to describe the locations of the point on the deformable body, a coordinate transformation that represents the orientation of the body coordinate systems with respect to an inertial frame is required to define the absolute position, velocity and acceleration. The use of this coordinate transformation leads to a highly nonlinear expression for the inertia forces and to a strong dynamic coupling between the absolute reference and local elastic coordinates [113]. But, the absolute nodal coordinate formulation uses isoparametric finite elements, which have the coordinates of each node defined in a fixed inertial coordinate system, to model the flexible bodies. Since no transformation matrices are required to define the kinematic position and velocity equations of the element, the expressions for the inertia forces are simple, but an expression for the elastic forces gets cumbersome [114]. The detailed review of the absolute nodal coordinate formulation is presented in [54,115]. Suppose the elastic forces are defined with respect to the local coordinate system using the linear theory of elasticity in the absolute nodal coordinate formulation. In that case, the method is equivalent to the sub-structuring techniques [116] used for the floating frame of reference formulation [12], in which each element corresponds to a substructure that undergoes large rotation and small deformation in order to account for the geometric nonlinearities. The method was adopted for modeling the geometrical stiffening in the rotating beam dynamics by many authors [117–119]. The effect of the centrifugal forces on the eigenvalue solution of nonlinear finite element formulations was examined by Maqueda et al. [120]. The authors compared the absolute nodal coordinate formulation with the formulation based on the geometrically exact beam theory, which assumes that the cross-section does not deform in its own plane and remains plane after deformation.

There are broadly three approaches in modeling the geometric stiffening effect in the dynamics of a rotating cantilever beam. The first approach directly provides axial centrifugal loads in the elastic energy expression. The time-independent centrifugal load can be obtained using any of the methods listed in Table 4. Mostly, the force is obtained by solving the equation governing the steady-state axial deformation. The second approach considers the longitudinal shrinkage caused by the transverse bending displacement corresponding to the foreshortening effect. The foreshortening effect is implicitly or explicitly included in the modeling based on the different strain measures used in the formulation. Implicit foreshortening methods are nonlinear and the equations are in terms of Cartesian variables u_i. However, explicit foreshortening methods are linear and the governing equations of motion are obtained in terms of a hybrid variable, for instance, stretch (s) or axial force, (EAs). The third approach uses an absolute nodal coordinate formulation mostly based on the finite element method [84,121–123].

3.3. Applicability of linear models

The solution of the steady state axial equilibrium equation Eq. (42),

$$u_{1s} = \frac{r\gamma\cos\big(\gamma(1-x)\big) + \sin(\gamma x)}{\gamma\cos(\gamma)} - (r+x),$$

is singular or diverges at critical angular velocity, $\gamma = \pi/2$. This has been reported as static instability of rotating beam at which the natural frequency becomes zero [92,94]. The critical value of the rotation speed appears to be the maximum limit for the structure and the previous authors referred to it as maximum angular velocity [76,94,124]. The expression for maximum steady strain at the fixed end (root, at $x = 0$) for a rotating uniform beam can be approximated as [48,76,91]

$$\epsilon_{max} = u'_{1s_{max}} = \gamma^2(r + 0.5). \tag{55}$$

In practice, the value of ϵ_{max} should not exceed yield strain. For most engineering materials, the yield strain is much smaller than unity. The angular velocity limit is defined based on the value of the maximum steady state axial strain at the root, which is close to the yield strain of the beam. To define the limit, the steady-state axial tip deformation and the axial root strain of an Euler–Bernoulli beam is plotted for different values of non-dimensional angular speed, $\gamma = \Omega\sqrt{\rho L^2/E}$, in Fig. 6. The solution of four steady-state axial equilibrium equations presented in the previous section are compared. The displacement and strain curves computed using the linear and nonlinear steady-state axial formulation begin to differ at the dimensionless angular velocity corresponding to an axial root strain of approximately 2% which is considered as maximum strain before structure failed. Solving for the dimensionless angular velocity corresponding to the maximum root strain of 2% yields the expression [48,76,94]

$$\gamma_{max} = \sqrt{\frac{0.02}{r + 0.5}}.$$

This expression can be used to compute the limit value of the angular speed of a rotating beam for which the structure is subject to sufficiently small strain so that a physically linear constitutive law applies. The value of $\gamma_{max} = 0.2$ for $r = 0$ at which the structure experiences the root strain higher than the structural limit imposed by yield stain. The instability predicted by the model based on the physically linear constitutive law occurs at an angular velocity $\gamma_{max} = \pi/2$, which is largely beyond the range where the strains can be correctly assumed to be small and structure sustain the large strain. Therefore, the study on the effect of the dimensionless rotation speed more than $\gamma = \Omega\sqrt{\rho L^2/E} > 0.2$ is not relevant from a practical point of view. The comparison study of the different steady-state axial equilibrium equations shows that the nonlinear and linear solutions give extremely close results before the structure fails (for $\gamma < 0.2$). Therefore, many previous authors used the linear model to compute the expression for the time-independent axial force. The solution of the Eq. (41) is the most suitable expression for steady-state axial motion owing to its simplicity and consistent accuracy in the lower range of rotation speed compared to the nonlinear model given in Eq. (43) or (44). The steady-state axial deformation and the axial strain of an Euler–Bernoulli beam along the beam length at a high rotation speed (higher than γ_{max}), $\gamma = 0.3$ are plotted in Fig. 7. The solution of all four steady-state axial equilibrium equations are extremely close

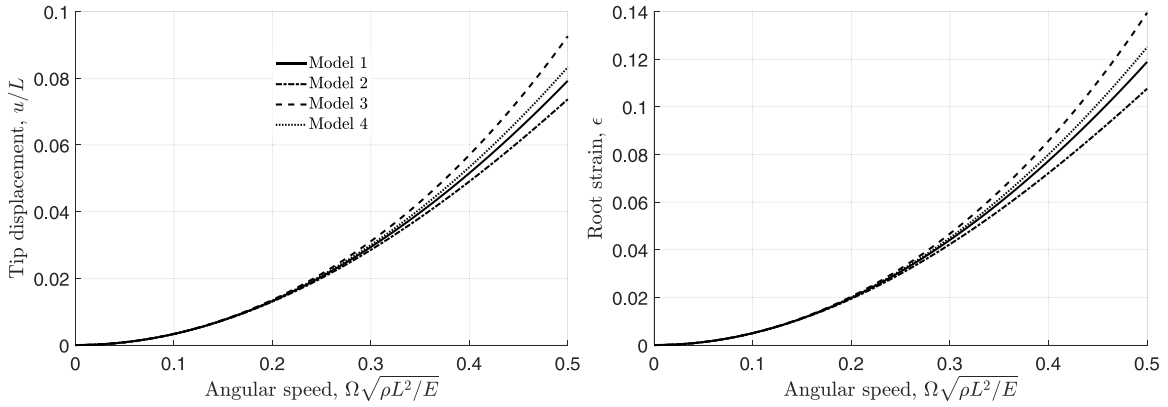

Fig. 6. Variation of the steady-state axial tip deformation and the axial root strain of an Euler–Bernoulli beam with nondimensional rotation speed (assume $r = 0$). The dash-dotted, dash, dotted and solid line represent the solution of Eq. (41), (42), (43) and (44), respectively.

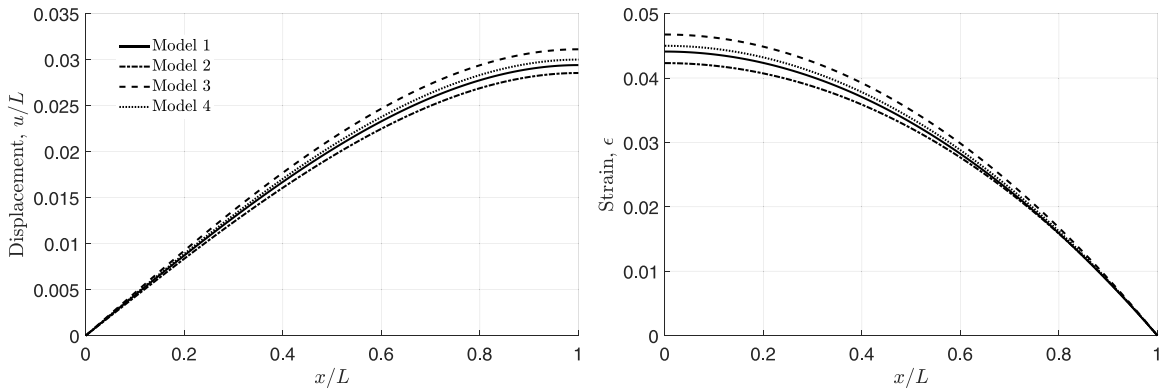

Fig. 7. The steady-state axial deformation and the axial strain of an Euler–Bernoulli beam at high rotation speed, $\gamma = 0.3$, were obtained by solving different equations governing the steady-state axial deformation with hub radius, $r = 0$. The dash-dotted, dash, dotted and solid line represent the solution of Eq. (41), (42), (43) and (44), respectively. The equations and corresponding solutions are summarized in Table 4.

at $\gamma = 0.3$. The study by Zhao and Wu [63] also concluded that the steady-state axial deformation causes significant changes in the transverse motion u_2 while influence is negligible on the other transverse motion, u_3. Also, the terms $3u'_{1s}u''_{1s}$ and $\frac{3}{2}u'^2_{1s}u''_{1s}$ in , arising from longitudinal quadratic term of the Green strain–displacement relationship, make an insignificant difference on the geometric stiffening effect of the rotating beam at lower speeds.

Some of the previous authors [91,94–96,98] observed that the first stretching natural frequency of the rotating Euler–Bernoulli beam becomes zero at a sufficiently high angular speed as shown in Fig. 8. The authors in [96] referred to the angular speed as buckling speed because the authors think the beam buckles at the zero natural frequency. The solution of the steady-state axial deformation equation given in Eq. (42) (refer row 3 in Table 4) become divergent at angular speed $\gamma = \pi/2$ which is the same as the buckling speed mentioned in [96]. However, the strain corresponding to the buckling speed $\epsilon_{max}\big|_{\gamma=\pi/2} = 2.9674$ (refer Eq. (55)) is largely beyond the range that the structure sustains. The instability predicted by the steady-state axial deformation model based on the physically linear constitutive law is largely beyond the range where the strains can be correctly assumed to be small. Interestingly, the buckling speed also corresponds to an angular velocity equal to the first axial natural frequency of a non-rotating beam [48].

Other researchers argued that though the axial stretching frequency decreases with increasing angular speed, it does not reduce to zero [63]. This is in line with the argument that the structure fails due to high root strain well before the frequency reduces to zero. It is clear from Fig. 6 that the maximum strain increases drastically with rotation speed and the structure fails because of the structural limit well below $\gamma = \pi/2$. The solution of Eq. (41) for $r = 0$ gives the relationship between the steady-state axial deformation and rotating speed as $u_{1s} = \frac{\gamma^2}{6}(3x - x^3)$ which indicate that the steady-state axial deformation rapidly increases with the increase in the rotating speed, so does the axial strain, $u'_{1s} = \frac{\gamma^2}{2}(1 - x^2)$. The expression for the rotating speed limit beyond which structure fails is given by

$$\Omega_c = \sqrt{2\sigma_c/\rho L^2},$$

where, σ_c elastic limit of the structure.

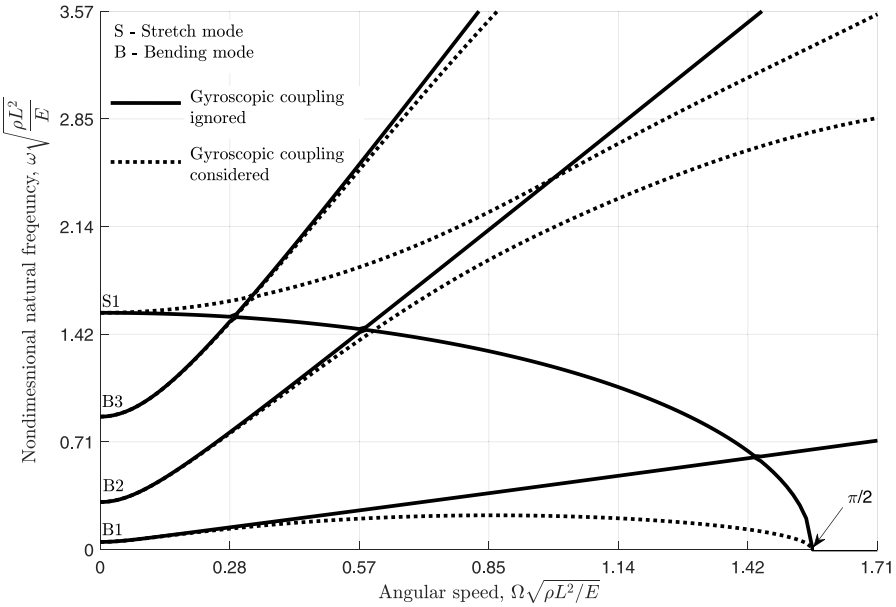

Fig. 8. Bending and stretch coupled natural frequencies of a rotating Euler–Bernoulli beam. Dotted and solid lines represent the natural frequencies obtained considering and ignoring the gyroscopic coupling between chord-wise and stretch motion, respectively.

To derive the expression for axial natural frequency, the axial vibration equation Eq. (34a) is considered ignoring the coupling with transverse motion,

$$\rho A(\ddot{u} - \Omega^2 u) - EAu'' = 0. \tag{56}$$

Using the assumed mode method, axial stretching natural frequency, ω_u, can be obtained as [63],

$$\omega_u = \sqrt{\frac{(2m-1)^2\pi^2}{4}\frac{E}{\rho L^2} - \Omega^2} = \sqrt{\omega_{u0}^2 - \Omega^2}, \quad m = 1, 2, 3, \ldots \tag{57}$$

where, ω_{u0} is the axial stretching natural frequency of the non-rotating beam. The equation shows that the axial stretching natural frequency decreases with increasing rotating speed. The axial stretching frequency should become zero when $\Omega = \omega_{u0}$. The axial natural frequency at the critical rotation speed limit, Ω_c can be expressed as

$$\begin{aligned}\omega_u &= \sqrt{\frac{E}{\rho}\frac{(2m-1)^2\pi^2}{4L^2} - \frac{2\sigma_c}{\rho L^2}} \\ &= \omega_{u0}\sqrt{1 - \frac{8}{(2m-1)^2\pi^2}\frac{\sigma_c}{E}}\end{aligned}$$

This indicates that the axial stretching natural frequency decreases with increasing rotating speed, but it is never reduced to zero because of the large difference between σ_c and E. As the values of m increases, ω_u becomes increasingly closer to ω_{u0}. Therefore, the effect of the rotating speed is smaller on higher modes of the stretching circular frequency.

It is concluded that the rotating speed decreases the magnitude of the natural frequency of the stretching mode when the effect of transverse motion on the axial vibration is not considered (Coriolis term). However, a decrease in the stretching frequency did not cause the chord-wise bending frequency to reduce to zero due to the structural limit at a critical rotating speed, Ω_c. Huang et al. [76] called Ω_c as the high angular velocity at which the structure loses its ability to resist steady-state axial strain due to centrifugal force. The high angular velocity is much lower than the speed at which the first bending natural frequency became zero. Invernizzi and Dozio [48] determined the angular velocity corresponding to a maximum axial strain closely equal to 2% (which indicates that the elongation is 2% of the length of the beam) for different values of the hub radius.

4. Formulation and solution approach

The equations of motion for the blade attached to a rotating hub fall in the class of problems generally referred to as a multi-body system, a collection of connected rigid bodies and deformable bodies, derived from various approaches. These approaches are broadly classified into two groups as the inertial frame of reference formulation and the floating frame of reference formulation based on the coordinate systems adopted to describe the motion [9,49]. *The inertial frame of reference formulation* uses a single global inertial

frame of reference to describe the movement of the system and the displacement of any point on the system is referred to this inertial system. Therefore, there is no distinction between rigid body motion and displacements due to deformation. Global displacements are discretized using finite-element method [95,125] or the finite difference method [126]. *The floating frame of reference formulation* uses global reference frame and local body reference frames associated with each body in the system to describe the motion. The configuration of the deformable body in the multibody system is identified by using two sets of coordinates: reference and elastic coordinates. Reference coordinates define the location and orientation of a selected body reference frame with a finite number of degrees of freedom. On the other hand, elastic coordinates describe the body deformation with respect to the body reference frame, which has an infinite number of degrees of freedom. The floating frame of reference formulation has been proved to be efficient in the analysis of large displacement/small deformation problems [84].

An introduction and background of different approximate solution approaches such as the Rayleigh method, Galerkin's method, and details of finite element method for a rotating beam problem are provided in books [127,128]. The most commonly adopted solution approach for rotating beam dynamics is modal approximation methods, the mode superposition method, or the assumed mode method. In the modal method, each continuous displacement variable is written as a weighted sum of a finite number of *basis functions*, each of which has a corresponding generalized modal coordinate that is a function of time only (variable separation). Basis functions are linearly independent and space-dependent functions. Based on the type of basis functions used, the modal method can be either *Galerkin's method* or *Rayleigh–Ritz method*. Galerkin's method first derives partial differential equations using Hamilton's principle and then performs the variable separation. The basis functions used in Galerkin's method should satisfy all boundary conditions (geometric boundary conditions on displacement and rotation and force boundary conditions on force and moment), usually called as *comparison functions*. Rayleigh–Ritz method is applied to Lagrange's equations or the principle of virtual work. The variable separation is performed for each continuous displacement variable in kinetic and potential energies and then derives ordinary differential equations using Lagrange's equations. The basis functions used in the Rayleigh–Ritz method should satisfy at least geometric boundary conditions, usually called as *admissible functions* [129]

For a rotating Euler–Bernoulli beam, the Galerkin and Rayleigh–Ritz method using the eigenfunctions of the non-rotating cantilever beam as basis functions are identical. This is because the Eigenfunctions are comparison functions for the Euler–Bernoulli beam that satisfy both geometric and force boundary conditions. The Galerkin method was used for the Euler–Bernoulli beam by many authors [24,75,86,108,130]. Some authors adopted the Rayleigh–Ritz method for rotating Euler–Bernoulli beam [6,96]

Some of the authors adopted the Galerkin method for a rotating Timoshenko beam [80]. However, using eigenfunctions of the non-rotating cantilever beam as basis functions for the Timoshenko beam, the Galerkin method will give inaccurate results. The eigenfunctions are admission functions for the Timoshenko beam, which satisfy only geometric boundary conditions. Therefore, most of the time Rayleigh–Ritz method is used for the Timoshenko beam using cantilever eigenfunctions as basis functions [110,131,132].

Finite element method (FEM) is a widely used solution method for rotating beam dynamics. FEM is based on the discretization of a structure into a large number of small elements, modeling them approximately, and connecting them together appropriately. Because of this way of discretizing the geometry, it is possible to accurately capture modeling details that other methods cannot [129]. Some authors adopted FEM for rotating Euler–Bernoulli beam [79,95,133] and for Timoshenko beam [70,73,84,134–137]. FEM is also used for tapered and twisted rotating blades [138]. Other methods derived from FEM and used for rotor dynamics are *Spectral FEM* [139,140] and *power series* [91].

Another method that is popular for the solution of rotor dynamics is *dynamic stiffness method* which is referred to as the exact method as it is based on exact shape functions obtained from the exact solution of the element differential equations [141,142]. The method is adopted for rotating uniform or tapered Euler–Bernoulli beam [97,98,101,143–145], tapered Rayleigh beam [146] and Timoshenko beam [91,100,147].

The differential transform method (DTM) was adopted for the rotating beam problem by Kaya and group, which is based on the Taylor series expansion. The method was adopted for a rotating tapered cantilever Bernoulli–Euler beam with linearly varying rectangular cross-section [148,149], axially loaded composite Timoshenko beam [149,150] and tapered Timoshenko beam [151].

5. Free vibration of rotating beam

Yoo and Shin [96] considered the dynamic characteristics of a uniform Euler–Bernoulli beam using the stretch variable. They derived the linear equations of motion governing the gyroscopically coupled stretching and chord-wise motion (u_2 motion) and uncoupled flap-wise motion (u_3 motion) (refer Fig. 5). The modal analysis was employed to calculate the natural frequencies of the rotating beam. The authors studied the effect of centrifugal force due to rotation and hub radius on the beam's natural frequency. It was observed that the third chord-wise motion and first stretching motion exhibit the veering phenomenon in which the loci of the eigenvalue come close to each other and veer away rather than cross. The authors computed the tuned angular speed, which results in resonance due to matching of the angular velocity with the beam's natural frequency. It was observed that the tuned angular velocity for the first mode existed in the chord-wise motion but did not exist in the flap-wise motion. Further, they concluded that the gyroscopic coupling due to Coriolis force between the stretching and chord-wise motion is insignificant at lower angular speeds and for highly slender beams. At the same time, the coupling effect is more substantial at a higher angular velocity, especially for lower modes. The effect of Coriolis force is to soften the bending mode and stiffen the stretch mode of a rotating beam. Hence the natural frequency of the first stretching mode increased in magnitude, whereas the first bending mode frequency was found to decrease with the angular speed. A similar conclusion was drawn by Lacarbonara et al. [152]. The Coriolis force that acts normal to the axial direction and opposite to the beam motion causes loss of tension which softens the beam in bending and decreases

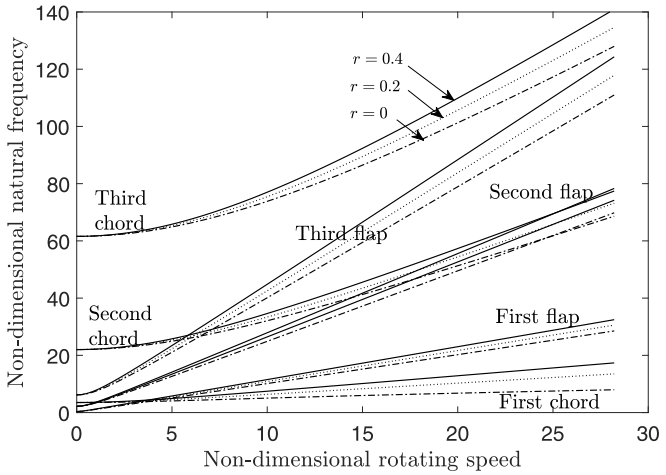

Fig. 9. Effect of hub radius on the natural frequencies of first three modes of flap-wise and chord-wise motion [155].

the natural bending frequency. However, this force stiffens the beam in axial motion, resulting in an increase in the stretch mode frequencies.

Further, the stretch-based linear modeling method was adopted by different authors for rotating beam applications. Yoo et al. [6] considered the pre-twisted Euler–Bernoulli rotating beam to investigate the natural frequency loci veering phenomena using the stretch variable. Zhu [110] adopted the non-Cartesian variable-based formulation to perform the modal analysis of a twisted beam, including the shear deformation effect. The author concluded that the slenderness ratio is the dominant parameter that affects the tuned angular speed in addition to the hub radius ratio. However, the veering phenomena observed by Yoo et al. [6] was not observed for a beam with shear deformation effects. Further, the study was extended for a rotating double-tapered beam by Zhu [111]. Oh and Yoo [131] performed the modal analysis of a rotating beam with an asymmetric cross-section. Using the linear dynamic model, the authors investigated the effect of the cross-section eccentricity, pre-twist angle and setting angle on the modal characteristics of the blade. They concluded that the cross-section asymmetry, pre-twist and presetting angle caused the veering phenomenon. The effort of previous researchers to understand the dynamics of the rotating beam reveals that there are various parameters such as taper, twist angle, asymmetric cross-section and presetting angle on which the modal characteristics of the beam depend. In the following two tables (Tables 5 and 6), a summary of the effect of each of the parameters is presented. In the following section, the effect of the geometry properties of the rotating blade on its modal characteristics is presented.

Hub radius

The effect of hub radius was investigated initially by Boyce et al. [153] and later by Lo et al. [154]. The perturbation method was applied to determine the change in the natural bending frequency with a change in hub radius. The study concluded that a frequency parameter of a beam is a linear function of the hub-radius change and the constant of proportionality is readily obtainable from known parameters. The variation of the dimensionless natural frequency with dimensionless speed for three different values of hub radius, r, is given in Fig. 9. The dimensionless natural frequencies increase as the dimensionless angular speed increases, and the increasing rates (the slope of the trajectory) become larger as the hub radius ratio becomes larger.

Pre-twist angle

The initial investigations of the rotating blade considered a uniform blade without a pre-twist. But, in reality, the blade can be twisted, which causes the coupling between the bending modes. A comprehensive review of the dynamic analysis of twisted beam is presented by Rosen [156]. Dawson and Carnegie [157] examined the effect of a pre-twist angle on the natural frequency of cantilever beams. Gupta and Rao [138] adopted an approximate method (the Ritz–Galerkin method) and the numerical method (FEM) to investigate the effects of pre-twist angle on the dynamic characteristics of a blade. Young [158] considered a pre-twisted blade resulting in coupling between the two bending modes of vibration. The free vibration characteristics of the twisted rotating beams, including the effect of transverse shear and rotary inertia, were investigated by several researchers [42,159–161]. The dynamic response of a rotating cantilever twisted Timoshenko beam constrained at the hub in a centrifugal force field is studied by Sinha [162]. Sinha observed a slight increase in the bending frequencies and a rapid decrease in the torsional frequency with the increasing twist. Hu et al. [42] studied the free vibration characteristics of a rotating cantilever conical shell with pre-twist, which is a model of turbomachinery blade. The author considered a blade with different thicknesses and presetting angles and investigated the effect of twist angle on the natural frequency. The author concluded that the twist angle decreases the fundamental frequency

Table 5
Effect of blade geometry and higher order effects on the modal characteristics.

	Causes	Effects	Ref.
Rotation effect			
Coriolis force	Gyroscopic coupling between the axial and the lag-wise (Chord-wise) motion.	Coupling of high frequency axial and low frequency bending motion results in numerical issues Softening effect on the chord-wise motion that reduces the natural frequency Geometrical stiffening effect on the axial motion and frequency increases with rotation speed. No effect on the flap-wise bending and torsion motion The coupling effect is significant at high rotation speeds.	[20,93,95,96,98,163–165]
Centrifugal force	Centrifugal stiffening effect on all modes (without gyroscopic coupling) Softening effect on axial motion with gyroscopic coupling	The frequencies of bending (chord-wise and flap-wise) and torsional motions increase with rotation speed and axial motion decreases with rotation speed when the gyroscopic coupling is considered	[48,63,75,76,86,87,89,90,92,93,95–101]
Geometric properties			
Hub radius	Increases the stiffening effect	A frequency of a blade is a linear function of the hub radius change	[95,96,98,100,135,147,150,153,154,166–168]
Taper	Considerable change in the distribution of mass and the stiffness along the blade length	The breadth taper ratio affects all the natural modes and the height taper ratio affects only the fundamental vibration mode	[111,148,149,169–173]
Twist angle	The coupling between the bending modes (flap-wise and chord-wise motion)	The fundamental frequency decrease with twist angle and the twist angle's influence is reduced at a higher rotation speed as a centrifugal force of rotation may cause deformation against the pre-twist The veering phenomena occurs due to pretwist and the existence of tuned angular velocity in the bending modes	[6,42,125,134,138,156–162,174]
Asymmetric cross-section	Due to offset along the principal axis between the elastic axis and the centroidal axis, the bending and torsional modes are coupled under the combined twisting and bending deformation of the blade	The bending frequencies decrease, and torsional frequencies increase with asymmetry. The asymmetry has a relatively dominating effect on higher modes	[87,131,132,136,143,175]
Pre-setting angle	Causes the coupling between axial and flap-wise bending, axial and torsional motion and bending–torsional motions	Increase the chord-wise and torsional mode frequencies and the effect is relatively more predominant in the fundamental mode	[97,132,163,166,176–178]
Higher order effects			
Shear deformation and Rotary inertia	For blades with smaller slenderness ratios and moderately large rotations, the higher order effects are significant	The natural frequencies decrease The effects are more significant for higher natural frequencies	[137,138,160,168,175,179,180]

and the twist angle's influence is reduced at a higher rotation speed. This could be because a centrifugal force of rotation may cause deformation against the pre-twist. The thin conical shell was more sensitive to the twist angle than the thick one.

Banerjee [160] investigated a twisted Timoshenko beam undergoing free natural vibration with the application of the dynamic stiffness matrix. The results concluded that the shear deformation and rotatory inertia have similar effects on the natural frequencies of a twisted beam as they have on an untwisted beam. Yoo et al. [6] considered the pre-twisted Euler–Bernoulli rotating beam to investigate the natural frequency loci veering phenomena using the stretch variable. Equations governing the two bending modes, i.e., chord-wise and flap-wise, coupled due to the pre-twist angle, were used for the computations. The authors showed manifestation of the veering phenomena caused by the pre-twist angle and tuned angular velocity in the first two bending modes. Furthermore, the authors elaborated on the effect of the pre-twist angle and the hub radius on the tuned angular velocity. Yardimoglu and Inman [125,134] considered a problem with an asymmetric cross-section of the blade in addition to the pre-twist resulting in coupling between the two bending modes and the torsional mode of vibration. They developed a FE model for the blade vibration, the results of which were compared with an experimental result conducted on the 250 MW turbine blade by Montoya [174].

Asymmetric cross section

The transverse and lateral bending vibrations are coupled with the torsional vibration due to asymmetry. The bending vibration that occurs in the plane perpendicular to the symmetry axis is coupled with the torsional vibration for only one symmetry axis [87,131,132,136,143,175]

Table 6
Study of rotating blade using different beam theories including different higher order effects.

Modeling details		Rotation effect		Geometrical properties			other effects
Beam theory	Solution approach	Hub radius	Coriolis force	Taper	Twist angle	Asymmetric cross-section	Pre-setting angle
Euler–Bernoulli beam	Rayleigh–Ritz method	[96,167]	[20,93, 96]	[163,181]	[171,181–186]	[176,182]	[176]
	Galerkin method	[166]	[164]				[166,177]
	Finite element method	[95,135, 167]	[95,165]	[139,140]	[135]	[165,187,188] [187]	[97]
	Dynamic stiffness method	[98,147]	[98]	[147]			[144]
	Other		[76,189]				
Rayleigh beam	Rayleigh–Ritz method			[155,190]	[155]		
	Galerkin method						
	Finite element method						
	Dynamic stiffness method	[146]					
	Other	[191,192]	[191,192]	[193]			
Timoshenko beam	Rayleigh–Ritz method	[132,178]	[132,178]		[110,132, 175,178, 194]	[132,178]	[132,178]
	Galerkin method						
	Finite element method	[168]	[168,175, 180]	[137,138, 168]	[137,138, 138,156, 195,196]	[137,175,180, 197]	
	Dynamic stiffness method	[100]			[160]		
	Other	[100,150]	[91,97, 198,199]	[151,173, 200,201]	[41,200, 202]	[200–202]	[97]

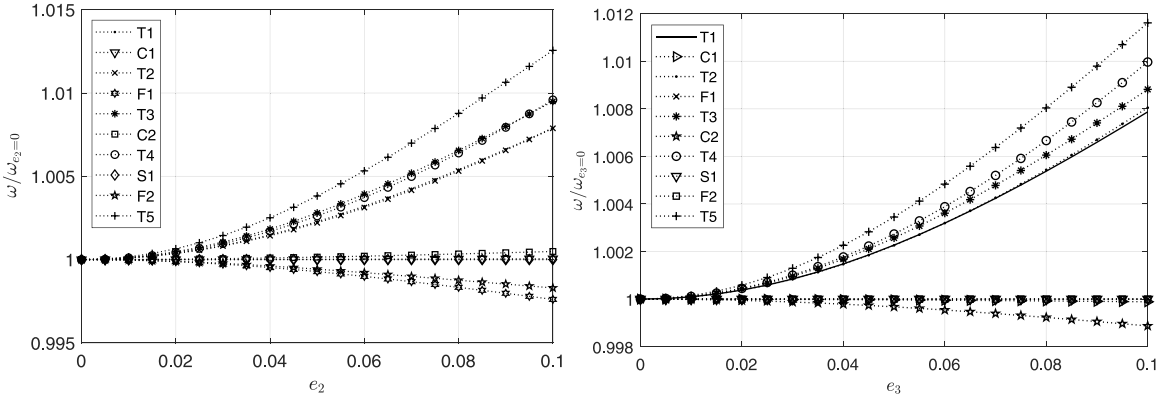

(a) Effect of e_2 (b) Effect of e_3

Fig. 10. Effect of the cross-section asymmetry on the natural frequency. F, C, T and S indicate the modes of flap-wise motion, chord-wise motion, torsional motion and stretch motion, respectively. The integer associated with each mode indicates the corresponding modal index [203].

Variation of the first nine non-dimensional natural frequencies with the non-dimensional rotation speed for a blade with an asymmetric cross-section (e_2 and e_2 are asymmetry in $\hat{a}_2$ and $\hat{a}_3$ direction, respectively) is given in Fig. 10. It is observed from the figure that the bending frequencies decreases and torsional frequencies increase with the extent of asymmetry. The asymmetry has a relatively dominating effect on the higher modes

Presetting angle

Variation of three fundamental frequencies of flap-wise, chord-wise and torsional motion is plotted against nondimensional rotating speed for different values of pre-setting angle in Fig. 11. In the figure, the ordinate represents the ratio of blade frequency with a pre-setting angle to the frequency of the blade without setting the angle. The pre-setting angle increases the chord-wise and torsional mode frequencies and the effect is relatively more dominant in the first mode.

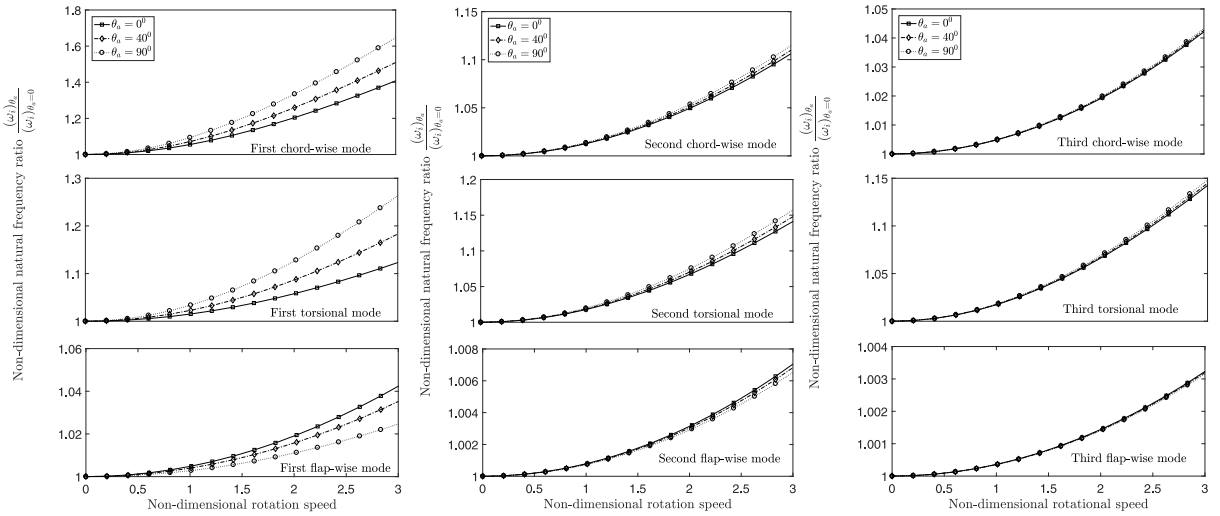

(a) Mode-1 (b) Mode-2 (c) Mode-3

Fig. 11. Variation of first three modes of flap-wise, chord-wise and torsional natural frequencies with non-dimensional rotation speed for different pre-setting angle [203].

Taper

The modal characteristics of a tapered blade often vary from those of uniform blades due to considerable changes in the distribution of mass and the stiffness along the blade length [169]. Downs [170] presented the natural frequencies of cantilever tapered beams. Subrahmanyam and Rao [171] determined the modal characteristics of a pre-twisted tapered blade using the Reissner method. Lee and Lin [172] investigated a rotating non-uniform beam using a semi-exact numerical method. Further, the study was extended to a rotating double-tapered beam by Zhu [111]. The study revealed that the breadth taper ratio affects all the natural modes and the height taper ratio affects only the fundamental vibration mode. The authors studied the influence of the taper ratio on the natural bending frequencies. Özdemir and Kaya [149] developed the differential transform method (DTM) to study the flexural vibration of a double-tapered beam. Further, the authors applied the DTM to analyze the flap-wise vibration of an Euler–Bernoulli beam [148] and Timoshenko beam [173]. Zhu [111] analyzed the transverse vibration of a rotating, double-tapered Timoshenko beam using the hybrid deformation variables.

Higher order effect

Four beam theories viz., Euler–Bernoulli, Rayleigh, shear and Timoshenko are analyzed for the transversely vibrating uniform beam [179]. The effect of shear deformation and rotary inertia is demonstrated for different beam boundary conditions. Banerjee [160] investigated a Timoshenko beam to study the effect of shear deformation and rotary inertia on the rotating beam with and without pre-twist. The results indicate that the natural frequencies decrease when the effects of shear deformation and rotatory inertia are considered. The effects are more significant for higher natural frequencies and smaller slenderness ratios. The effects of shear deformation and rotatory inertia on the natural frequencies of a twisted beam are similar to those of an untwisted beam. However, the effects are seen to be marginally more pronounced in the case of a twisted beam than that of an untwisted one. The summary of the study on rotating beam dynamics is provided in Table 6

6. Conclusion

A detailed review of the modeling methods to account for the geometrical stiffening effect induced by rotation in the blade is presented. The kinematic description and then expression for strain and kinetic energies of a rotating blade modeled using a beam is developed for the most general case. Subsequently, the geometrically exact model for the blade undergoing large deformation and small strain is discussed through a consistent linearization procedure. Then models for geometrical stiffening models are presented. The modeling methods can be either explicit or implicit based on how the foreshortening effect is incorporated into the kinematics description of the blade motion. In the implicit method, the geometrical stiffening terms are nonlinear, arising from coupled axial-bending motion. Such a method requires considering many high-frequency axial modes in the solution procedure, making it inefficient. It is possible to linearize the implicit model to study the geometrical stiffening effect. Various linear implicit models are presented and compared to each other for applicability for a range of rotation speeds. The explicit modeling method

is based on the stretch variable, which measures the blade elongation using coordinates after deformation. The stretch variable includes the foreshortening effect explicitly in the kinematic description. It was concluded that the explicit modeling method is more accurate and computationally inexpensive. Also, the convergence of the explicit method is much better than the implicit method. Different solution procedures are discussed in the context of the rotating blade. The results of the explicit model obtained using the assumed mode method are comparable to those of the implicit model using the finite element procedure. Therefore, the appropriate method should be chosen based on the nature of the governing equations and boundary conditions. The implicit model has nonlinear boundary conditions, and it is challenging to find the base functions that satisfy such boundary conditions for the assumed mode solution method. However, the explicit model has linear boundary conditions hence the assumed method can be used with base functions for the corresponding boundary conditions. The rotation effect on the blade has two folds: a centrifugal stiffening and a gyroscopic coupling effect. For a rotating beam, it was observed that the bending motion and the stretch motion exhibit the veering phenomenon in which the loci of the eigenvalue come close to each other and veer away rather than cross. The effect of Coriolis force is to soften the bending mode and stiffen the stretch mode of a rotating beam.

Data availability

No data was used for the research described in the article.

References

[1] J. Rao, Turbomachine Blade Vibration, New Age International, 1991.
[2] O. Wallrapp, R. Schwertassek, Representation of geometric stiffening in multibody system simulation, Internat. J. Numer. Methods Engrg. 32 (8) (1991) 1833–1850.
[3] F. Vigneron, Comment on “mathematical modeling of spinning elastic bodies for modal analysis”, AIAA J. 13 (1) (1975) 126–127.
[4] K. Kaza, R. Kvaternik, Nonlinear flap-lag axial equations of a rotating beam, AIAA J. 15 (6) (1977) 871–874.
[5] T. Kane, R. Ryan, A. Banerjee, Dynamics of a cantilever beam attached to a moving base, J. Guid. Control Dyn. 10 (2) (1987) 139–151.
[6] H. Yoo, J. Park, J. Park, Vibration analysis of rotating pre-twisted blades, Comput. Struct. 79 (19) (2001) 1811–1819.
[7] J. May, J. Dominguez, A. Shabana, Geometrically nonlinear formulations of beams in flexible multibody dynamics, J. Vib. Acoust. 117 (4) (1995) 501–509.
[8] I. Sharf, Geometric stiffening in multibody dynamics formulations, J. Guid. Control Dyn. 18 (4) (1995) 882–890.
[9] J. Mayo, D. García-Vallejo, J. Domínguez, Study of the geometric stiffening effect: comparison of different formulations, Multibody Syst. Dyn. 11 (4) (2004) 321–341.
[10] P. Likins, F. Barbera, V. Baddeley, Mathematical modeling of spinning elastic bodies for modal analysis, AIAA J. 11 (9) (1973) 1251–1258.
[11] J. Simo, L. Vu-Quoc, The role of non-linear theories in transient dynamic analysis of flexible structures, J. Sound Vib. 119 (3) (1987) 487–508.
[12] S. Wu, E. Haug, Geometric non-linear substructuring for dynamics of flexible mechanical systems, Internat. J. Numer. Methods Engrg. 26 (10) (1988) 2211–2226.
[13] A. Leissa, Vibrational aspects of rotating turbomachinery blades, Appl. Mech. Rev. 34 (5) (1981) 629–635.
[14] V. Ramamurti, P. Balasubramanian, Analysis of turbomachine blades: a review, Shock Vib. Digest 16 (3) (1984) 13–28.
[15] A. Leissa, J. Lee, A. Wang, Vibrations of twisted rotating blades, J. Vib. Acoust. Stress Reliab. Des. 106 (2) (1984) 251–257.
[16] D. Kunz, Survey and comparison of engineering beam theories for helicopter rotor blades, J. Aircr. 31 (3) (1994) 473–479.
[17] A. Bazoune, Survey on modal frequencies of centrifugally stiffened beams, Shock Vib. Digest 37 (6) (2005) 449–469.
[18] M. Rafiee, F. Nitzsche, M. Labrosse, Dynamics, vibration and control of rotating composite beams and blades: A critical review, Thin-Walled Struct. 119 (2017) 795–819.
[19] B.T. Murphy, Eigenvalues of rotating machinery (stability, rotor dynamics, vibration) (Ph.D. thesis), Texas A&M University, 1984.
[20] J. Chimin, Coriolis effects on the vibrations of rotating beams, plates and shells (Ph.D. thesis), The Ohio State University, 1984.
[21] A. Bazoune, Vibration frequencies of rotating tapered beam including rotary inertia and transverse shear deformation (Ph.D. thesis), King Fahd University of Petroleum and Minerals (Saudi Arabia), 1990.
[22] C.D. Eick, Free vibration of flexible rotating beams and plates (Ph.D. thesis), Arizona State University, 1994.
[23] O. Thomas, A. Sénéchal, J.-F. Deü, Hardening/softening behavior and reduced order modeling of nonlinear vibrations of rotating cantilever beams, Nonlinear Dynam. 86 (2) (2016) 1293–1318.
[24] H. Kim, J. Chung, Nonlinear modeling for dynamic analysis of a rotating cantilever beam, Nonlinear Dynam. 86 (3) (2016) 1981–2002.
[25] D. Hodges, Review of composite rotor blade modeling, AIAA J. 28 (3) (1990) 561–565.
[26] S. Jung, V. Nagaraj, I. Chopra, Assessment of composite rotor blade modeling techniques, J. Am. Helicopter Soc. 44 (3) (1999) 188–205.
[27] L. Librescu, O. Song, Thin-Walled Composite Beams: Theory and Application, Springer Science & Business Media, 2005.
[28] D.H. Hodges, Nonlinear Composite Beam Theory, American Institute of Aeronautics and Astronautics, 2006.
[29] M. Ghorashi, Statics and Rotational Dynamics of Composite Beams, Springer, 2016.
[30] S. Oh, L. Librescu, O. Song, Vibration of turbomachinery rotating blades made-up of functionally graded materials and operating in a high temperature field, Acta Mech. 166 (1) (2003) 69–87.
[31] L. Li, D. Zhang, W. Zhu, Free vibration analysis of a rotating hub–functionally graded material beam system with the dynamic stiffening effect, J. Sound Vib. 333 (5) (2014) 1526–1541.
[32] J. Tian, Z. Zhang, H. Hua, Free vibration analysis of rotating functionally graded double-tapered beam including porosities, Int. J. Mech. Sci. 150 (2019) 526–538.
[33] H. Arvin, S. Hosseini, Y. Kiani, Free vibration analysis of pre/post buckled rotating functionally graded beams subjected to uniform temperature rise, Thin-Walled Struct. 158 (2021) 107187.
[34] M. Filippi, D. Giusa, A. Pagani, E. Zappino, E. Carrera, Assessment of classical, advanced, and layer-wise theories for the vibration of rotating composite anisotropic blades, Compos. Struct. 245 (2020) 112315.
[35] F. Bekhoucha, S. Rechak, L. Duigou, J. Cadou, Nonlinear forced vibrations of rotating anisotropic beams, Nonlinear Dynam. 74 (4) (2013) 1281–1296.
[36] A. Leissa, J. MacBain, R. Kielb, Vibrations of twisted cantilevered plates-summary of previous and current studies, J. Sound Vib. 96 (2) (1984) 159–173.
[37] M. Dokainish, S. Rawtani, Vibration analysis of rotating cantilever plates, Internat. J. Numer. Methods Engrg. 3 (2) (1971) 233–248.
[38] H. Yoo, S. Kim, Free vibration analysis of rotating cantilever plates, AIAA J. 40 (11) (2002) 2188–2196.
[39] T. Young, G. Liou, Coriolis effect on the vibration of a cantilever plate with time-varying rotating speed, J. Vib. Acoust. 114 (2) (1992) 232–241.
[40] A. Leissa, M. Ewing, Comparison of beam and shell theories for the vibrations of thin turbomachinery blades, J. Eng. Power 105 (2) (1983) 383–392.
[41] Y. Kee, J. Kim, Vibration characteristics of initially twisted rotating shell type composite blades, Compos. Struct. 64 (2) (2004) 151–159.

[42] X. Hu, T. Sakiyama, H. Matsuda, C. Morita, Fundamental vibration of rotating cantilever blades with pre-twist, J. Sound Vib. 271 (1–2) (2004) 47–66.
[43] H. Kang, C. Chang, H. Saberi, R. Ormiston, Assessment of beam and shell elements for modeling rotorcraft blades, J. Aircr. 51 (2) (2014) 520–531.
[44] E. Díaz, 3D Motion of Rigid Bodies, Springer, 2019.
[45] P. Pai, Highly Flexible Structures: Modeling, Computation, and Experimentation, American Institute of Aeronautics and Astronautics, 2007.
[46] O. Bauchau, Flexible Multibody Dynamics, Springer, 2011.
[47] A. Nayfeh, P. Frank, Linear and Nonlinear Structural Mechanics, John Wiley & Sons, 2008.
[48] D. Invernizzi, L. Dozio, A fully consistent linearized model for vibration analysis of rotating beams in the framework of geometrically exact theory, J. Sound Vib. 370 (2016) 351–371.
[49] A. Shabana, Dynamics of Multibody Systems, Cambridge University Press, 2020.
[50] H. El-Absy, A.A. Shabana, Geometric stiffness and stability of rigid body modes, J. Sound Vib. 207 (4) (1997) 465–496.
[51] Q. Li, T. Wang, X. Ma, A note on the foreshortening effect of a flexible beam under oblique excitation, Multibody Syst. Dyn. 23 (2) (2010) 209–225.
[52] W. Gau, A. Shabana, Effects of shear deformation and rotary inertia on the nonlinear dynamics of rotating curved beams, J. Vib. Acoust. 112 (2) (1990) 183–193.
[53] J. Reddy, An Introduction to Nonlinear Finite Element Analysis Second Edition: With Applications to Heat Transfer, Fluid Mechanics, and Solid Mechanics, OUP Oxford, 2014.
[54] J. Gerstmayr, H. Sugiyama, A. Mikkola, Review on the absolute nodal coordinate formulation for large deformation analysis of multibody systems, J. Comput. Nonlinear Dyn. 8 (3) (2013).
[55] A. Schwab, J.P. Meijaard, Comparison of three-dimensional flexible beam elements for dynamic analysis: classical finite element formulation and absolute nodal coordinate formulation, J. Comput. Nonlinear Dyn. 5 (1) (2010).
[56] J. Gerstmayr, M.K. Matikainen, A.M. Mikkola, A geometrically exact beam element based on the absolute nodal coordinate formulation, Multibody Syst. Dyn. 20 (4) (2008) 359–384.
[57] T. Hughes, K. Pister, Consistent linearization in mechanics of solids and structures, Comput. Struct. 8 (3–4) (1978) 391–397.
[58] J. Thomsen, Vibrations and Stability: Advanced Theory, Analysis, and Tools, Springer Science & Business Media, 2013.
[59] M.C. Da Silva, D. Hodges, Nonlinear flexure and torsion of rotating beams, with application to helicopter rotor blades-I. Formulation, Vertica 10 (2) (1986) 151–169.
[60] M.C. da Silva, D. Hodges, Nonlinear flexure and torsion of rotating beams, with application to helicopter rotor blades-II. Response and stability results, Vertica 10 (2) (1986) 171–186.
[61] J. Warminski, L. Kloda, S. Lenci, Nonlinear vibrations of an extensional beam with tip mass in slewing motion, Meccanica 55 (12) (2020) 2311–2335.
[62] J. González-Carbajal, A. Rincón-Casado, D. García-Vallejo, J. Domínguez, Nonlinear solutions for the steady state oscillations of a clamped–free rotating beam, Eur. J. Mech. A Solids 91 (2022) 104413.
[63] G. Zhao, Z. Wu, Coupling vibration analysis of rotating three-dimensional cantilever beam, Comput. Struct. 179 (2017) 64–74.
[64] I. Sharf, Geometrically non-linear beam element for dynamics simulation of multibody systems, Internat. J. Numer. Methods Engrg. 39 (5) (1996) 763–786.
[65] J. Piedbœuf, B. Moore, On the foreshortening effects of a rotating flexible beam using different modeling methods, Mech. Struct. Mach. 30 (1) (2002) 83–102.
[66] J. Mayo, J. Dominguez, Geometrically non-linear formulation of flexible multibody systems in terms of beam elements: Geometric stiffness, Comput. Struct. 59 (6) (1996) 1039–1050.
[67] U. Lugrís, M. Naya, J. Pérez, J. Cuadrado, Implementation and efficiency of two geometric stiffening approaches, Multibody Syst. Dyn. 20 (2) (2008) 147–161.
[68] G. Zhao, J. Du, Z. Wu, A geometric softening phenomenon of a rotating cantilever beam, Arch. Appl. Mech. 87 (6) (2017) 1049–1059.
[69] H. Arvin, F. Bakhtiari-Nejad, Non-linear modal analysis of a rotating beam, Int. J. Non-Linear Mech. 46 (6) (2011) 877–897.
[70] P. Apiwattanalunggarn, S. Shaw, C. Pierre, D. Jiang, Finite-element-based nonlinear modal reduction of a rotating beam with large-amplitude motion, J. Vib. Control 9 (3–4) (2003) 235–263.
[71] F. Wang, Model reduction with geometric stiffening nonlinearities for dynamic simulations of multibody systems, Int. J. Struct. Stab. Dyn. 30 (08) (2013) 135–146.
[72] D. Hodges, R. Ormiston, Nonlinear equations for bending of rotating beams with application to linear flap-lag stability of hingeless rotors, NASA Technical Memorandum X-2770, 1973.
[73] S. Stoykov, P. Ribeiro, Vibration analysis of rotating 3D beams by the p-version finite element method, Finite Elem. Anal. Des. 65 (2013) 76–88.
[74] Y. Zhou, Y. Zhang, G. Yao, Nonlinear forced vibration analysis of a rotating three-dimensional tapered cantilever beam, J. Vib. Control 27 (15–16) (2021) 1879–1892.
[75] H. Kim, H. Yoo, J. Chung, Dynamic model for free vibration and response analysis of rotating beams, J. Sound Vib. 332 (22) (2013) 5917–5928.
[76] C. Huang, W. Lin, K. Hsiao, Free vibration analysis of rotating Euler beams at high angular velocity, Comput. Struct. 88 (17–18) (2010) 991–1001.
[77] E. Pesheck, C. Pierre, S. Shaw, Modal reduction of a nonlinear rotating beam through nonlinear normal modes, J. Vib. Acoust. 124 (2) (2002) 229–236.
[78] P. Roy, S. Meguid, Analytical modeling of the coupled nonlinear free vibration response of a rotating blade in a gas turbine engine, Acta Mech. 229 (8) (2018) 3355–3373.
[79] Z. Liu, J. Hong, J. Liu, Finite element formulation for dynamics of planar flexible multi-beam system, Multibody Syst. Dyn. 22 (1) (2009) 1–26.
[80] Y. Huo, Z. Wang, Dynamic analysis of a rotating double-tapered cantilever timoshenko beam, Arch. Appl. Mech. 86 (6) (2016) 1147–1161.
[81] R. Valembois, P. Fisette, J. Samin, Comparison of various techniques for modelling flexible beams in multibody dynamics, Nonlinear Dynam. 12 (4) (1997) 367–397.
[82] P. Shi, J. McPhee, G. Heppler, A deformation field for Euler–Bernoulli beams with applications to flexible multibody dynamics, Multibody Syst. Dyn. 5 (1) (2001) 79–104.
[83] S. Ider, F. Amirouche, Nonlinear modeling of flexible multibody systems dynamics subjected to variable constraints, J. Appl. Mech. 56 (2) (1989) 444–450.
[84] M. Berzeri, A. Shabana, Study of the centrifugal stiffening effect using the finite element absolute nodal coordinate formulation, Multibody Syst. Dyn. 7 (4) (2002) 357–387.
[85] A. Banerjee, J. Dickens, Dynamics of an arbitrary flexible body in large rotation and translation, J. Guid. Control Dyn. 13 (2) (1990) 221–227.
[86] J. Yang, L. Jiang, D. Chen, Dynamic modelling and control of a rotating Euler–Bernoulli beam, J. Sound Vib. 274 (3–5) (2004) 863–875.
[87] M. Kaya, O. Ozgumus, Energy expressions and free vibration analysis of a rotating uniform timoshenko beam featuring bending—torsion coupling, J. Vib. Control 16 (6) (2010) 915–934.
[88] E. Pesheck, C. Pierre, S. Shaw, Accurate reduced-order models for a simple rotor blade model using nonlinear normal modes, Math. Comput. Modelling 33 (10–11) (2001) 1085–1097.
[89] H. Lim, H. Yoo, Modal analysis of a multi-blade system undergoing rotational motion, J. Mech. Sci. Technol. 23 (8) (2009) 2051–2058.
[90] A. Al-Qaisia, B. Al-Bedoor, Evaluation of different methods for the consideration of the effect of rotation on the stiffening of rotating beams, J. Sound Vib. 280 (3–5) (2005) 531–553.
[91] S. Lin, K. Hsiao, Vibration analysis of a rotating Timoshenko beam, J. Sound Vib. 240 (2) (2001) 303–322.
[92] D. Hodges, R. Bless, Axial instability of rotating rods revisited, Int. J. Non-Linear Mech. 29 (6) (1994) 879–887.

[93] X. Yang, Z. Li, W. Zhang, T. Yang, Tian-Zhi, C. Lim, On the gyroscopic and centrifugal effects in the free vibration of rotating beams, J. Vib. Control 25 (1) (2019) 219–227.
[94] F. Bekhoucha, S. Rechak, L. Duigou, J. Cadou, Nonlinear free vibrations of centrifugally stiffened uniform beams at high angular velocity, J. Sound Vib. 379 (2016) 177–190.
[95] J. Chung, H. Yoo, Dynamic analysis of a rotating cantilever beam by using the finite element method, J. Sound Vib. 249 (1) (2002) 147–164.
[96] H. Yoo, S. Shin, Vibration analysis of rotating cantilever beams, J. Sound Vib. 212 (5) (1998) 807–828.
[97] S. Hashemi, M. Richard, Natural frequencies of rotating uniform beams with coriolis effects, J. Vib. Acoust. 123 (4) (2001) 444–455.
[98] J. Banerjee, D. Kennedy, Dynamic stiffness method for inplane free vibration of rotating beams including Coriolis effects, J. Sound Vib. 333 (26) (2014) 7299–7312.
[99] W. Zhu, C. Mote(Jr), Dynamic modeling and optimal control of rotating Euler–Bernoulli beams, J. Dyn. Syst. Meas. Control 119 (4) (1997) 802–808.
[100] J. Banerjee, Dynamic stiffness formulation and free vibration analysis of centrifugally stiffened Timoshenko beams, J. Sound Vib. 247 (1) (2001) 97–115.
[101] J. Banerjee, Free vibration of centrifugally stiffened uniform and tapered beams using the dynamic stiffness method, J. Sound Vib. 233 (5) (2000) 857–875.
[102] J. Mayo, J. Dominguez, A finite element geometrically nonlinear dynamic formulation of flexible multibody systems using a new displacements representation, J. Vib. Acoust. 119 (4) (1997) 573–581.
[103] J. Liu, J. Hong, Geometric stiffening effect on rigid-flexible coupling dynamics of an elastic beam, J. Sound Vib. 278 (4–5) (2004) 1147–1162.
[104] M.C. da Silva, C. Glynn, Nonlinear flexural-flexural-torsional dynamics of inextensional beams. I. Equations of motion, J. Struct. Mech. 6 (4) (1978) 437–448.
[105] M.C. da Silva, C. Glynn, Nonlinear flexural-flexural-torsional dynamics of inextensional beams. II. Forced motions, J. Struct. Mech. 6 (4) (1978) 449–461.
[106] P. Pai, A. Nayfeh, Non-linear non-planar oscillations of a cantilever beam under lateral base excitations, Int. J. Non-Linear Mech. 25 (5) (1990) 455–474.
[107] H. Yoo, R. Ryan, R. Scott, Dynamics of flexible beams undergoing overall motions, J. Sound Vib. 181 (2) (1995) 261–278.
[108] S. Seo, H. Yoo, Dynamic analysis of flexible beams undergoing overall motion employing linear strain measures, AIAA J. 40 (2) (2002) 319–326.
[109] H. Yoo, S. Lee, S. Shin, Flapwise bending vibration analysis of rotating multi-layered composite beams, J. Sound Vib. 286 (4–5) (2005) 745–761.
[110] T. Zhu, The vibrations of pre-twisted rotating Timoshenko beams by the Rayleigh–Ritz method, Comput. Mech. 47 (4) (2011) 395–408.
[111] T. Zhu, Free flapewise vibration analysis of rotating double-tapered Timoshenko beams, Arch. Appl. Mech. 82 (4) (2012) 479–494.
[112] S. Kwon, J. Chung, H. Yoo, Structural dynamic modeling and stability of a rotating blade under gravitational force, J. Sound Vib. 332 (11) (2013) 2688–2700.
[113] M. Berzeri, M. Campanelli, A.A. Shabana, Definition of the elastic forces in the finite-element absolute nodal coordinate formulation and the floating frame of reference formulation, Multibody Syst. Dyn. 5 (1) (2001) 21–54.
[114] J. Escalona, H. Hussien, A. Shabana, Application of the absolute nodal co-ordinate formulation to multibody system dynamics, J. Sound Vib. 214 (5) (1998) 833–851.
[115] K. Otsuka, K. Makihara, H. Sugiyama, Recent advances in the absolute nodal coordinate formulation: Literature review from 2012 to 2020, J. Comput. Nonlinear Dyn. 17 (8) (2022) 080803.
[116] J. Valverde, D. García-Vallejo, Stability analysis of a substructured model of the rotating beam, Nonlinear Dynam. 55 (4) (2009) 355–372.
[117] X. Zhang, D. Zhang, S. Chen, J. Hong, Modal characteristics of a rotating flexible beam with a concentrated mass based on the absolute nodal coordinate formulation, Nonlinear Dynam. 88 (1) (2017) 61–77.
[118] Y. Chen, D. Zhang, L. Li, Dynamics analysis of a rotating plate with a setting angle by using the absolute nodal coordinate formulation, Eur. J. Mech. A Solids 74 (2019) 257–271.
[119] Y. Chen, D. Zhang, L. Li, Dynamic analysis of rotating curved beams by using absolute nodal coordinate formulation based on radial point interpolation method, J. Sound Vib. 441 (2019) 63–83.
[120] L.G. Maqueda, O.A. Bauchau, A.A. Shabana, Effect of the centrifugal forces on the finite element eigenvalue solution of a rotating blade: a comparative study, Multibody Syst. Dyn. 19 (3) (2008) 281–302.
[121] M. Berzeri, A. Shabana, Development of simple models for the elastic forces in the absolute nodal co-ordinate formulation, J. Sound Vib. 235 (4) (2000) 539–565.
[122] A. Nada, B. Hussein, S. Megahed, A. Shabana, Use of the floating frame of reference formulation in large deformation analysis: experimental and numerical validation, Proc. Inst. Mech. Eng. K 224 (1) (2010) 45–58.
[123] A. Shabana, R. Schwertassek, Equivalence of the floating frame of reference approach and finite element formulations, Int. J. Non-Linear Mech. 33 (3) (1998) 417–432.
[124] J. Gunda, R. Gupta, R. Ganguli, Hybrid stiff-string–polynomial basis functions for vibration analysis of high speed rotating beams, Comput. Struct. 87 (3–4) (2009) 254–265.
[125] B. Yardimoglu, D. Inman, Coupled bending-bending-torsion vibration of a pre-twisted beam with aerofoil cross-section by the finite element method, Shock Vib. 10 (4) (2003) 223–230.
[126] W. Carnegie, J. Thomas, The effects of shear deformation and rotary inertia on the lateral frequencies of cantilever beams in bending, J. Eng. Ind. 94 (1) (1972) 267–278.
[127] R. Ganguli, Finite Element Analysis of Rotating Beams: Physics Based Interpolation, Springer Verlag, Singapore, 2018.
[128] R. Ganguli, V. Panchore, The Rotating Beam Problem in Helicopter Dynamics, Springer, 2018.
[129] D. Hodges, G. Pierce, Introduction to Structural Dynamics and Aeroelasticity, Cambridge University Press, 2011.
[130] L. Li, W. Zhu, D. Zhang, C. Du, A new dynamic model of a planar rotating hub–beam system based on a description using the slope angle and stretch strain of the beam, J. Sound Vib. 345 (2015) 214–232.
[131] Y. Oh, H. Yoo, Vibration analysis of a rotating pre-twisted blade considering the coupling effects of stretching, bending, and torsion, J. Sound Vib. 431 (2018) 20–39.
[132] X. Wu, Y. Jiao, Z. Chen, An analytical model of a rotating radial cantilever beam considering the coupling between bending, stretching, and torsion, J. Vib. Acoust. 144 (2) (2021).
[133] J. Gunda, R. Ganguli, New rational interpolation functions for finite element analysis of rotating beams, Int. J. Mech. Sci. 50 (3) (2008) 578–588.
[134] B. Yardimoglu, D. Inman, Coupled bending-bending-torsion vibration of a rotating pre-twisted beam with aerofoil cross-section and flexible root by finite element method, Shock Vib. 11 (5–6) (2004) 637–646.
[135] D. Hodges, M. Rutkowski, Free-vibration analysis of rotating beams by a variable-order finite element method, AIAA J. 19 (11) (1981) 1459–1466.
[136] M. Mohiuddin, Y. Khulief, Coupled bending torsional vibration of rotors using finite element, J. Sound Vib. 223 (2) (1999) 297–316.
[137] S. Rao, R. Gupta, Finite element vibration analysis of rotating Timoshenko beams, J. Sound Vib. 242 (1) (2001) 103–124.
[138] S. Gupta, S. Rao, Finite element eigenvalue analysis of tapered and twisted Timoshenko beams, J. Sound Vib. 56 (2) (1978) 187–200.
[139] G. Wang, N. Wereley, Free vibration analysis of rotating blades with uniform tapers, AIAA J. 42 (12) (2004) 2429–2437.
[140] K. Vinod, S. Gopalakrishnan, R. Ganguli, Free vibration and wave propagation analysis of uniform and tapered rotating beams using spectrally formulated finite elements, Int. J. Solids Struct. 44 (18–19) (2007) 5875–5893.
[141] J. Banerjee, Dynamic stiffness formulation for structural elements: a general approach, Comput. Struct. 63 (1) (1997) 101–103.
[142] T. Liu, J. Lin, Forced vibration of flexible body systems: A dynamic stiffness method, J. Vib. Acoust. 115 (4) (1993) 468–476.

[143] W. Hallauer Jr., R. Liu, Beam bending-torsion dynamic stiffness method for calculation of exact vibration modes, J. Sound Vib. 85 (1) (1982) 105–113.
[144] K. Huang, T. Liu, Dynamic analysis of rotating beams with nonuniform cross sections using the dynamic stiffness method, J. Vib. Acoust. 123 (4) (2001) 536–539.
[145] R. Firouz-Abadi, H. Haddadpour, An asymptotic solution to transverse free vibrations of variable-section beams, J. Sound Vib. 304 (3–5) (2007) 530–540.
[146] J. Banerjee, D. Jackson, Free vibration of a rotating tapered Rayleigh beam: a dynamic stiffness method of solution, Comput. Struct. 124 (2013) 11–20.
[147] J. Banerjee, H. Su, D. Jackson, Free vibration of rotating tapered beams using the dynamic stiffness method, J. Sound Vib. 298 (4–5) (2006) 1034–1054.
[148] Ö. Özdemir, M. Kaya, Flapwise bending vibration analysis of a rotating tapered cantilever Bernoulli–Euler beam by differential transform method, J. Sound Vib. 289 (1–2) (2006) 413–420.
[149] M. Kaya, O. Ozgumus, Flapwise bending vibration analysis of double tapered rotating Euler–Bernoulli beam by using the differential transform method, Meccanica 41 (6) (2006) 661–670.
[150] C. Mei, Differential transformation approach for free vibration analysis of a centrifugally stiffened timoshenko beam, J. Vib. Acoust. 128 (2) (2005) 170–175.
[151] O. Ozgumus, M. Kaya, Vibration analysis of a rotating tapered Timoshenko beam using DTM, Meccanica 45 (1) (2010) 33–42.
[152] W. Lacarbonara, H. Arvin, F. Bakhtiari-Nejad, A geometrically exact approach to the overall dynamics of elastic rotating blades—part 1: linear modal properties, Nonlinear Dynam. 70 (1) (2012) 659–675.
[153] W.E. Boyce, Effect of hub radius on the vibrations of a uniform bar, J. Appl. Mech. 2 (23) (1956) 287–290.
[154] H. Lo, J. Goldberg, J. Bogdanoff, Effect of small hub-radius change on bending frequencies of a rotating beam, J. Appl. Mech. 3 (27) (1960) 548–550.
[155] L. Hoskoti, A. Misra, M. M. Sucheendran, Modal analysis of a rotating twisted and tapered Rayleigh beam, Arch. Appl. Mech. 91 (6) (2021) 2535–2567.
[156] A. Rosen, Structural and dynamic behavior of pretwisted rods and beams, Appl. Mech. Rev. 44 (12) (1991) 483–515.
[157] B. Dawson, W. Carnegie, Modal curves of pre-twisted beams of rectangular cross-section, J. Mech. Eng. Sci. 11 (1) (1969) 1–13.
[158] T. Young, Dynamic resppnse of a pretwisted, tapered beam with non-constant rotating speed, J. Sound Vib. 150 (3) (1991) 435–446.
[159] S.M. Lin, Dynamic analysis of rotating nonuniform timoshenko beams with an elastically restrained root, Appl. Mech. Rev. 66 (3) (1999) 742–749.
[160] J. Banerjee, Development of an exact dynamic stiffness matrix for free vibration analysis of a twisted Timoshenko beam, J. Sound Vib. 270 (1–2) (2004) 379–401.
[161] C. Chen, S. Ho, Transverse vibration of a rotating twisted Timoshenko beams under axial loading using differential transform, Int. J. Mech. Sci. 41 (11) (1999) 1339–1356.
[162] S. Sinha, Combined torsional-bending-axial dynamics of a twisted rotating cantilever timoshenko beam with contact-impact loads at the free end, J. Appl. Mech. 74 (3) (2007) 505–522.
[163] K. Subrahmanyam, K. Kaza, Vibration and buckling of rotating, pretwisted, preconed beams including coriolis effects, J. Vib. Acoust. Stress Reliab. Des. 108 (2) (1986) 140–149.
[164] J. Tian, J. Su, K. Zhou, H. Hua, A modified variational method for nonlinear vibration analysis of rotating beams including coriolis effects, J. Sound Vib. 426 (2018) 258–277.
[165] F. Sisto, A. Chang, A finite element for vibration analysis of twisted blades based on beam theory, AIAA J. 22 (11) (1984) 1646–1651.
[166] C. Yang, S. Huang, Coupling vibrations in rotating shaft-disk-blades system, J. Vib. Acoust. 129 (1) (2007) 48–57.
[167] H. Lee, Vibration on an inclined rotating cantilever beam with tip mass, J. Vib. Acoust. 115 (3) (1993) 241–245.
[168] A. Bazoune, Y. Khulief, N. Stephen, M. Mohiuddin, Dynamic response of spinning tapered Timoshenko beams using modal reduction, Finite Elem. Anal. Des. 37 (3) (2001) 199–219.
[169] A. Bazoune, Y. Khulief, N. Stephen, Further results for modal characteristics of rotating tapered Timoshenko beams, J. Sound Vib. 219 (1) (1999) 157–174.
[170] B. Downs, Transverse vibrations of cantilever beams having unequal breadth and depth tapers, J. Appl. Mech. 44 (4) (1977) 737–742.
[171] K. Subrahmanyam, J. Rao, Coupled bending-bending vibrations of pretwisted tapered cantilever beams treated by the Reissner method, J. Sound Vib. 82 (4) (1982) 577–592.
[172] S. Lee, Y. Kuo, Bending vibrations of a rotating non-uniform beam with an elastically restrained root, J. Sound Vib. 154 (3) (1992) 441–451.
[173] Ö. Özdemir, M. Kaya, Flapwise bending vibration analysis of a rotating double-tapered Timoshenko beam, Arch. Appl. Mech. 78 (5) (2008) 379–392.
[174] J. Montoya, Coupled bending and torsional vibrations in a twisted rotating blade, Brown Boveri Rev. 53 (3) (1966) 216–230.
[175] K. Subrahmanyam, S. Kulkarni, J. Rao, Coupled bending-bending vibrations of pre-twisted cantilever blading allowing for shear deflection and rotary inertia by the Reissner method, Int. J. Mech. Sci. 23 (9) (1981) 517–530.
[176] W. Carnegie, Vibrations of rotating cantilever blading: theoretical approaches to the frequency problem based on energy methods, J. Mech. Eng. Sci. 1 (3) (1959) 235–240.
[177] J. Rao, W. Carnegie, Solution of the equations of motion of coupled-bending bending torsion vibrations of turbine blades by the method of Ritz-Galerkin, Int. J. Mech. Sci. 12 (10) (1970) 875–882.
[178] H. Heydari, A. Khorram, L. Afzalipour, The influences of stagger and pretwist angles of blades on coupling vibration in shaft-disk-blade systems, J. Vib. Acoust. 142 (1) (2019).
[179] S. Han, H. Benaroya, T. Wei, Dynamics of transversely vibrating beams using four engineering theories, J. Sound Vib. 225 (5) (1999) 935–988.
[180] M. Sabuncu, K. Evran, Dynamic stability of a rotating pre-twisted asymmetric cross-section Timoshenko beam subjected to an axial periodic force, Int. J. Mech. Sci. 48 (6) (2006) 579–590.
[181] W. Carnegie, J. Thomas, The coupled bending—bending vibration of pre-twisted tapered blading, J. Manuf. Sci. Eng. 94 (1) (1972) 255–266.
[182] W. Carnegie, Vibrations of pre-twisted cantilever blading, Proc. Inst. Mech. Eng. 173 (1) (1959) 343–374.
[183] D. Rosard, Natural frequencies of twisted cantilever beams, J. Appl. Mech. 20 (2) (2021) 241–244.
[184] H. Slyper, Coupled bending vibrations of pretwisted cantilever beams, J. Mech. Eng. Sci. 4 (4) (1962) 365–379.
[185] B. Dawson, Coupled bending-bending vibrations of pre-twisted cantilever blading treated by the Rayleigh–Ritz energy method, J. Mech. Eng. Sci. 10 (5) (1968) 381–388.
[186] J. Wu, B. Titurus, Modal analysis of a rotating pre-twisted beam axially loaded by an internally guided tendon, J. Sound Vib. 498 (2021) 115980.
[187] W. Carnegie, B. Dawson, Vibration characteristics of pre-twisted blades of asymmetrical aerofoil cross-section, Aeronaut. Q. 22 (3) (1971) 257–273.
[188] V. Ramamurti, R. Kielb, Natural frequencies of twisted rotating plates, J. Sound Vib. 97 (3) (1984) 429–449.
[189] F. Sisto, A. Chang, M. Sutcu, The influence of coriolis forces on gyroscopic motion of spinning blades, J. Eng. Power 105 (2) (1983) 342–347.
[190] R. Ganesh, R. Ganguli, Stiff string approximations in Rayleigh–Ritz method for rotating beams, Appl. Math. Comput. 219 (17) (2013) 9282–9295.
[191] A. Yigit, A. Ulsoy, R. Scott, Dynamics of a radially rotating beam with impact, part 1: Theoretical and computational model, J. Vib. Acoust. 112 (1) (1990) 65–70.
[192] A. Yigit, A. Ulsoy, R. Scott, Dynamics of a radially rotating beam with impact, part 2: Experimental and simulation results, J. Vib. Acoust. 112 (1) (1990) 71–77.
[193] A. Tang, X. Li, J. Wu, K. Lee, Flapwise bending vibration of rotating tapered Rayleigh cantilever beams, J. Construct. Steel Res. 112 (2015) 1–9.
[194] W. Carnegie, Vibrations of pre-twisted cantilever blading allowing for rotary inertia and shear deflection, J. Mech. Eng. Sci. 6 (2) (1964) 105–109.
[195] Z. Celep, D. Turhan, On the influence of pretwisting on the vibration of beams including the shear and rotatory inertia effects, J. Sound Vib. 110 (3) (1986) 523–528.
[196] W. Chen, L. Keer, Transverse vibrations of a rotating twisted Timoshenko beam under axial loading, J. Vib. Acoust. 115 (3) (1993) 285–294.

[197] J. Thomas, M. Sabuncu, Finite element analysis of rotating pretwisted asymmetric cross-section blades, in: American Society of Mechanical Engineers, Design Engineering Technical Conference, Vol. 10, (12) 1979.
[198] M. Ansari, N. Jalili, Exact frequency analysis of a rotating cantilever beam with tip mass subjected to torsional-bending vibrations, J. Vib. Acoust. 133 (4) (2011).
[199] L. B. Fallahiand S, R. Gupta, Full beam formulation of a rotating beam-mass system, J. Vib. Acoust. 116 (1) (1994) 93–99.
[200] W. Carnegie, J. Thomas, The effects of shear deformation and rotary inertia on the lateral frequencies of cantilever beams in bending, J. Eng. Ind. 94 (1) (1972) 267–278.
[201] O. Ozgumus, M. Kaya, Energy expressions and free vibration analysis of a rotating double tapered Timoshenko beam featuring bending–torsion coupling, Internat. J. Engrg. Sci. 45 (2–8) (2007) 562–586.
[202] C. Fu, Computer analysis of a rotating axial-turbomachine blade in coupled bending-bending-torsion vibrations, Internat. J. Numer. Methods Engrg. 8 (3) (1974) 569–588.
[203] L. Hoskoti, S. S. Gupta, M. M. Sucheendran, Rotation-induced geometrical stiffening of a tapered, pretwisted blade, AIAA J. (2022) 1–27.